iScience

CellPress
OPEN ACCESS

Article

Deciphering trophic interactions in a mid-Cambrian assemblage

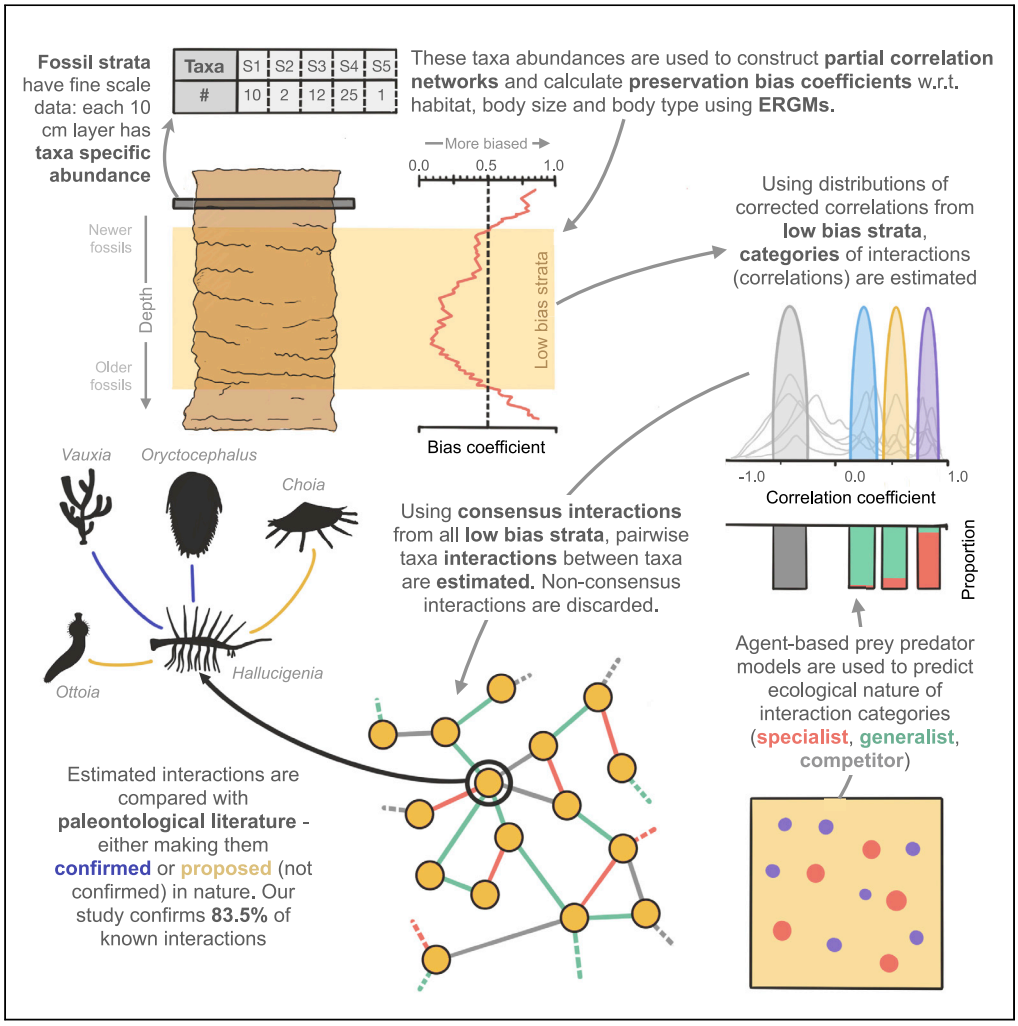

Anshuman Swain, Matthew Devereux, William F. Fagan

answain@terpmail.umd.edu

Highlights

Network analysis of well-preserved fossil communities can predict probable interactions

Clustering analyses of these interactions reveal possible ecological categories

Agent-based models can help infer/map these categories to known ecological patterns

High agreement of predictions to hypothesized trophic interactions from literature

Swain et al., iScience 24, 102271
April 23, 2021
https://doi.org/10.1016/j.isci.2021.102271

iScience

CellPress
OPEN ACCESS

Article

Deciphering trophic interactions in a mid-Cambrian assemblage

Anshuman Swain,[1,3,*] Matthew Devereux,[2] and William F. Fagan[1]

SUMMARY

Exceptionally preserved fossil sites have allowed specimen-based identification of trophic interactions to which network analyses have been applied. However, network analyses of the fossil record suffer from incomplete and indirect data, time averaging that obscures species coexistence, and biases in preservation. Here, we present a high-resolution fossil data set from Raymond Quarry member of the mid-Cambrian Burgess Shale (7,549 specimens, 61 taxa, ~510 Mya) and formulate a measure of "preservation bias" that aids identification of assemblage subsets to which network analyses can be reliably applied. For these sections, abundance correlation network analyses predicted longitudinally consistent trophic and competitive interactions. Our analyses predicted previously postulated trophic interactions with 83.5% accuracy and demonstrated a shift from specialist interaction-dominated assemblages to ones dominated by generalist and competitive interactions. This approach provides a robust, taphonomically corrected framework to explore and predict in detail the existence and ecological character of putative interactions in fossil data sets.

INTRODUCTION

Evolutionarily, the Cambrian Period (541–485 Mya) is unique because it witnessed the emergence and rapid diversification of phylum-level extant animal body plans and featured the highest morphological and genetic rates of animal evolution (Erwin et al., 2011; Lee et al., 2013). Morphological disparity and behavioral complexity increased (Seilacher et al., 2005; Carbone and Narbonne, 2014), prompting hypotheses about major shifts in ecological interactions and trophic structure during this period, due to major changes such as widespread predation and active (vertical) burrowing, which may have facilitated the first complex "modern" food webs (Morris, 1986; Vannier and Chen, 2005; Dunne et al., 2008; Erwin and Valentine, 2012; Mángano and Buatois, 2014). "Conservation lagerstätten" sedimentary deposits, featuring exceptional fossil preservation of both "soft" and "hard" body features (Orr et al., 2003), permit detailed studies from which species interactions can be deduced (Butterfield, 2003). Previous works have focused on these well-preserved Cambrian localities for performing detailed paleoecological analyses and have contributed immensely to our understanding of the Cambrian ecosystem (Caron and Jackson, 2006; Caron and Jackson, 2008; Zhao et al., 2014) However, network-based approaches can provide new perspectives, helping to resolve ongoing debates and shedding new light on community structure.

Network-based studies provide critical insight on the structure and function of ecological systems (Ings et al., 2009; Poisot et al., 2016; Delmas et al., 2017), but paleo-assemblages often suffer from incomplete and indirect data (Roopnarine, 2010; Shaw et al., 2021), time-averaging across large stratigraphic sections that obscure species coexistence (Kidwell et al., 1991; Dunne et al., 2008; Roopnarine, 2010; Muscente et al., 2018), and biases in preservation, collection, and identification of both specimens and interactions (Koch, 1978; Smith, 2001; Dunne et al., 2008). Although some previous network studies have been performed on almost census preserved communities, such as in the Ediacaran (Mitchell and Butterfield, 2018; Mitchell et al., 2019; Muscente et al., 2019). Here, we report an extensive mid-Cambrian fossil abundance data set featuring excellent preservation with high stratigraphic resolution, consistent taxa presence, and low biases in collection and identification. Using partial correlation network analyses of fossil abundance data and agent-based models, we find statistical evidence recapitulating 71 of 85 previously known or suspected species interactions, propose 117 previously unknown putative interactions, and identify a shift from assemblages dominated by specialist interactions to ones dominated by

[1]Department of Biology, University of Maryland, College Park, MD 20742, USA

[2]Department of Earth Science, Western University, London, ON, Canada

[3]Lead contact

*Correspondence: answain@terpmail.umd.edu

https://doi.org/10.1016/j.isci.2021.102271

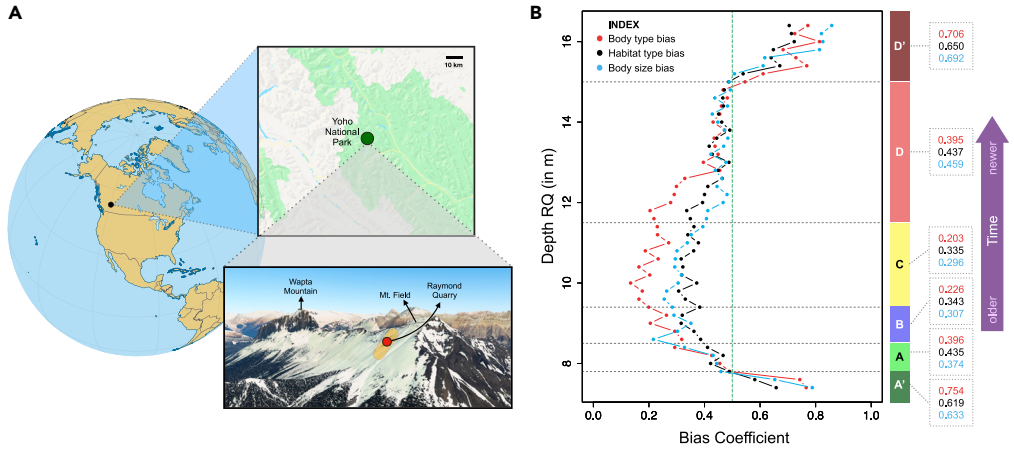

Figure 1. Location, biofacies, and bias

(A) Location of Raymond Quarry (RQ) (Yoho National Park, BC, Canada), denoted by red dot; yellow region denotes extent of major Burgess Shale localities; samples were collected from the RQ member along the "fossil ridge" connecting Mt. Field and Wapta Mountain. (Figure S1 and methods) (B) "Preservation bias coefficient" for body type (with respect to soft, intermediate, and hard bodied categorization) (in red), habitat type (in black), and body size categories (in blue) calculated using networks in running time frame analysis, plotted along with estimated boundaries for the distinct sub-assemblages (A-D) in the 9.3 m shale section using variations of two different statistical approaches for biofacies detection: ANOSIM and SHEBI (Figure S2 and methods) and the associated average bias coefficient for each sub-assemblage (in their respective index colors for each type of bias). The green dotted line depicts the bias threshold we adopted for inclusion versus exclusion of sample layers. Preservation bias coefficients exceeding 0.5 translate into substantial changes in the structure of interaction networks calculated from abundance correlations (Figure S3B). Note that the 10 cm layers comprising regions A′ and D′ were originally identified as belonging to sub-assemblages A and D, but fossils from A′ and D′ were not used in the analyses presented here because of evidence for high levels of preservation bias among taxa.

competition and generalized interactions. All results derive directly from fossil abundance data, without assuming any prior knowledge about species interactions.

Employing classic tools of network analysis, we characterize fine-scale structure and dynamics of the paleoecological system represented by a 7,549-specimen data set from the Raymond Quarry (RQ) of the Middle Cambrian Burgess Shale of SE BC, Canada (~510 Mya, Figures 1A; S1). This data set, which represents one of the most complete views of early animal assemblages, consists of species-wise abundance for 61 taxa in 10 cm levels across 9.3 m of shale. These Burgess Shale assemblages are thought to be the result of rapid entombment of fossils in fine-grained sediments (Gaines et al., 2012). Oxidant flow into sediments was prevented by the quick sealing of sediments by widespread carbonate cements (a result of highly alkaline Cambrian oceans), in an ocean where low sulfate and low-oxygen bottom waters already reduced oxidant concentration. This resulted in exceptional preservation of organisms and provided a unique fingerprint of the Cambrian. Interpretation of the details of the entombment and preservation processes differ among studies (Gaines et al., 2012; Schiffbauer et al., 2014; Sperling et al., 2018).

Previous network studies of paleontological data from the Burgess Shale (e.g., Dunne et al., 2008; Shaw et al., 2021) have focused on the Walcott Quarry, which is from the same geological period and has much higher species diversity than RQ but unlike RQ lacks consistent species preservation throughout its constituent bedding planes (Devereux, 2001). In addition, all RQ bedding planes were scanned thoroughly and fossils were identified and labeled immediately upon discovery in the field to nearest decimeter bedding plane, resulting in a low collection bias (for details, see methods). Therefore, this data set's fine-scale spatial resolution and the site's exceptional, consistent preservation of soft-bodied organisms allows us to assume representative population preservation throughout (most of) the assemblage and therefore offer advantages not available to most earlier paleo-assemblage network analyses (Dunne et al., 2008; Dormann et al., 2017). Moreover, in addition to usage of network methods, we utilized agent-based models to quantify and test key concerns, affording (a) a computational approach to understand preservation bias in fossil assemblages, (b) identification of putative interactions among taxa, (c) categorization of putative interactions into ecological roles, and (d) understanding of trophodynamics over time.

RESULTS AND DISCUSSION

Based on consensus results from two statistical approaches commonly used to define boundaries between fossil assemblages—SHEBI (Buzas and Hayek, 1998) and ANOSIM (Clarke and Warwick, 1994) (methods and Figures 1B; S2)—we identified four distinct sub-assemblages (named A-D in decreasing order of age), which match previous biofacies identification based on paleontologically defined trophic nuclei (Devereux, 2001). Based on these results, we calculated statistically corrected pairwise correlation of abundance for all taxa in each of the four sub-assemblages, and each of the 46 groupings of 20 cm levels organized to facilitate analyses at a finer stratigraphic resolution (hereafter referred to as the running time frame analysis; for the bulk of the analysis, we use these planes as constituents of the larger A-D layers/sub-assemblages, and for the "running time frame/finer stratigraphic resolution analysis", we used data at a smaller cross section of the entire sub-assemblage, again whose smallest unit is fossil abundance in 20 cm level stratigraphic bedding planes.) (methods). These correlations, with relevant regularization, were then used to construct correlation networks, for each sub-assemblage and each component of the running time frame analysis. In these networks, each node was a taxon and each edge between a node pair represented significant correlation and thus possible interaction (methods).

Correlation networks can yield insights into possible interactions among taxa (Zhang, 2011; Barberán et al., 2012; Carr et al., 2019), but network features can be obscured by preservation and collection biases (Dunne et al., 2008; Jordano, 2016; Carr et al., 2019). Intensive sampling and detailed annotation reduced collection bias in this data set, but preservation bias can still yield altered patterns of abundance. Statistical corrections have addressed some issues of fossil preservation biases (Mitchell, 2015; Starrfelt and Liow, 2016; Flannery Sutherland et al., 2019), but these have not targeted applications involving network analyses. Moreover, previous work has shown that despite these biases, abundance and rank abundance of species in the fossil record tends to have high fidelity (see Kidwell, 2001; Kowalewski et al., 2006).

Preservation bias can occur for several reasons, most notably presence/absence of hard body parts/biomineralizable structures (which aid preservation), body size (which determines amount of preservable material and often the size of populations), and location/habitat (which provide differential conditions for preservation). If two taxa are both well preserved, their true abundance correlation is expected to exhibit less noise than correlations among pairs of taxa in which at least one taxon is not well preserved. Differential preservation biases among taxa could introduce subtle structuring in a correlation-based network that would be biased toward more well-preserved taxa. The network-level consequences of such biases can be quantified by comparison with exponential random graph models (ERGMs), which have been used to understand the effects of bias and missing data (Robins et al., 2004).

To understand the influence of preservation bias on fossil correlation networks, we constructed an agent-based simulation model (ABM) of a complex resource-prey-predator system (consisting of 17 prey, 8 predators, and a common base resource for prey; methods). We ran 1 million simulations of this ABM that differed in various initial conditions, such as starting population size of each species and average resource density. For each of the 1 million simulations, we then created 100 cases, where each of the component species was assigned independently to one of three categories differentiated by probability of preservation (methods), and also retained the corresponding base case in which each species had perfect preservation (i.e., the original abundance data). For all 101 million cases (100 million cases with modified preservation and the corresponding 1 million original cases with perfect preservation), we then calculated abundance correlations among species pairs and constructed regularized correlation networks. We formulated a bias coefficient, using ERGMs and Hamming distance, to capture the effect of differential preservation on network structure through pairwise analyses of corresponding cases with modified and perfect preservation (Figure S3, methods). Higher bias coefficients corresponded to greater alterations of network structure.

We then applied this bias coefficient to the fossil data in the running time frame analysis (methods). We separately considered three factors that could map onto differences in preservation: body type (hard bodied, partially hard bodied, soft bodied), body size (<15cm, 15–30 cm, and >30 cm maximum size), and habitat usage (endobenthic/epibenthic, nektobenthic, and nektonic/pelagic) (methods). Information on these factors was compiled from literature surveys: body type, maximum body size, and habitat usage (see Supplemental Information and, Royal Ontario Museum Database).

For all three factors, we found evidence for significant differential preservation bias at the start and the end of the collected assemblage in regions A′ and D′ that were, respectively, originally part of sub-assemblages A and D identified through biofacies detection (Figure 1B). Because of their heightened preservation bias, which was strong enough to substantially alter apparent network structure, data from regions A′ and D′ were excluded from further analyses. In contrast, we found low levels of preservation bias coefficients in each of the defined sub-assemblages (A-D), with respect to body type, body size, and habitat (Figure 1B; bias coefficient was <0.5 for all cases; methods). These preservation biases were low enough to have inconsequential effects on network structure (Figures 1B and S3). The three preservation bias coefficient series (shown in Figure 1B) are weakly correlated. This might be due to the fact that the number of specimens affects our ERGM values, and in the beginning and the end of the data set, we see low number of total specimens per level. One would expect heightened levels of preservation bias at the beginning and end of a fossil bed if the strata above and below the sampled assemblage did not allow proper preservation of organisms due to a change in environmental (preservation) conditions (Orr et al., 2003). From a taphonomic viewpoint, factors such as differential transport experienced between taxa and between fossil beds, the degree of time averaging, and pre-burial transport distances may shape the preservation of discoverable assemblage contents as well (Olson et al., 1980; Martin, 1999). Consequently, complete preservation of all ecological information is seldom expected (Flannery Sutherland et al., 2019; Saleh et al., 2020). However, the consistency in low preservation bias coefficient with respect to body preservation type, habitat type, and body size throughout sub-assemblages A-D (with removal of A′ and D′ and corresponding running time frames) suggests that the net taphonomic effect resulted in an overall relatively homogeneous burial of a group of taxa across the whole assemblage (Figure 1B). Nevertheless, some loss of taxa may not have been inferable from the fossil data using our methods, and small differences in preservation may still be present throughout the assemblage at the taxon level.

Even though we report no significant preservation biases beyond those at the A′ and D′ ends of the RQ assemblage based on the predicted "in situ" preservation potential of the RQ taxa, the original interactions may still have been subjected to certain biases (Butterfield, 2003). However, these possibilities are not pertinently different than methodological biases affecting recent or extant ecological data (Dunne et al., 2008; Armitage and Jones, 2019).

Both experimental and theoretical studies predict that prey-predator abundances should be correlated on long time scales (Tobin and Bjørnstad, 2003; Liebhold et al., 2004; Blasius et al., 2020), and we found this to be true for our ABM simulations (Figure S4). This result supports the premise that fossil abundance correlations might correspond to potential species interactions, where the degree of preservation bias is low, such as in extremely well-preserved assemblages like the Burgess shale (Saleh et al., 2020) and census-like preservation of Ediacaran communities (Mitchell et al., 2019). Furthermore, the distribution of abundance correlations should characterize system-level interactions. For example, we might hypothesize that abundances of competitors should be negatively correlated, whereas abundances of species engaged in highly specialized interactions should be strongly positively correlated, assuming homogeneous transport and burial. The shape and location of the distribution of fossil abundance correlations differed among sub-assemblages A-D (Figure 2A and 2B). In particular, the frequency of small magnitude correlations and of negative correlations increased over time from A to D. Moreover, in addition to species interactions, these correlations can also be a result of habitat overlap or exclusivity (and other phenomena such as mutualisms, indirect environmental effects, etc.) even in the case of relatively homogeneous burial. Later in this work, we try to tease apart if habitat preferences had any effect on the correlation structure and found none.

To explore if changes in correlational distributions represented a shift in the dominant mode of species interaction over time, we decomposed the corrected correlation distribution for each sub-assemblage A-D, which were used in network construction, into its respective basis functions using maximum likelihood (methods). In each sub-assemblage A -D, the distribution of abundance correlations was best fit by a sum of four Gaussian distributions (Figure S6 and methods), and across sub-assemblages, the four Gaussians had similar means but different amplitudes and variances (Figure 2A). We found a similar result for the (finer stratigraphic resolution) running time frame analysis. To categorize these Gaussians in the correlations of fossil data into possible clusters, we calculated a pairwise similarity matrix of all the component Gaussians across the assemblage and then performed a spectral analysis with the "gap" statistic (Tibshirani et al., 2001; methods) on it, which revealed four clusters of Gaussians (Figures 2A and 2B; methods).

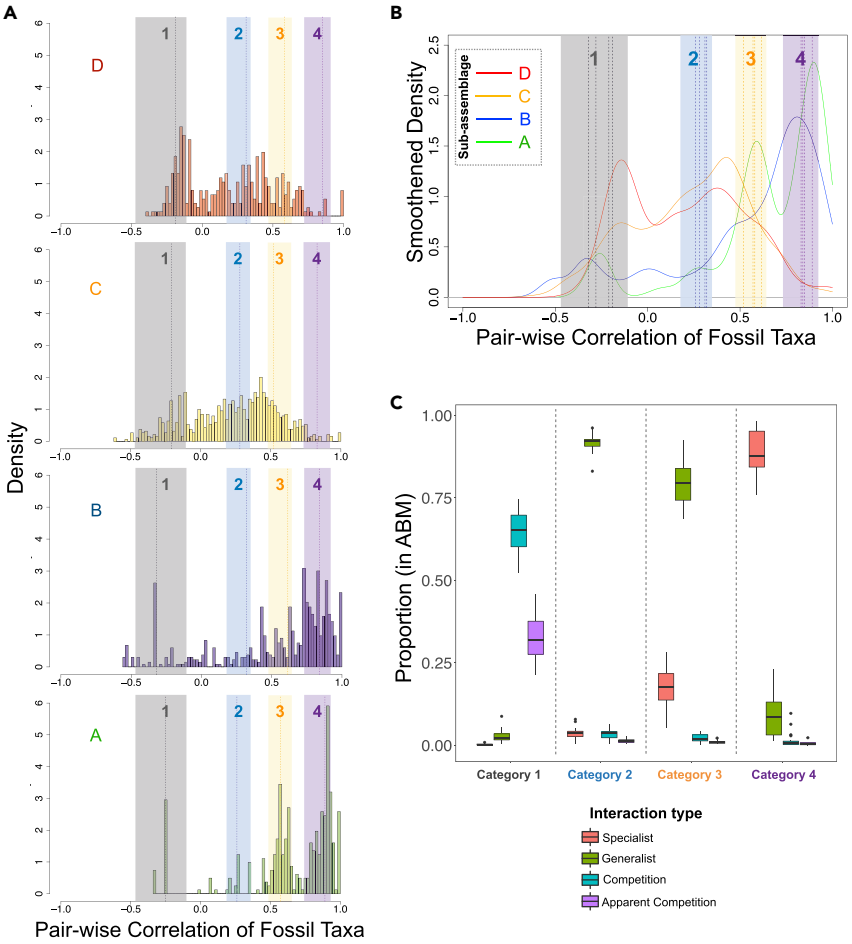

Figure 2. Characterization of interactions

(A) Distribution of pairwise correlations across A–D; dotted lines indicate the means of the basis Gaussians in each sub-assemblage calculated using maximum likelihood analysis for decomposing the abundance correlation distributions; colored bands indicate the four interaction categories 1–4, which represent the range of the Gaussian means for each interaction type, clustered from the basis Gaussians of the running time frame analysis using spectral analysis with gap statistics (see methods).

(B and C) (B) Summary of the four categories of interactions, calculated from spectral analysis, on the smoothened density distributions of pairwise correlation of fossils in the four sub-assemblages A–D; dotted lines indicate the means of Gaussian basis distributions from A–D; (C) Proportion of different feeding types in the ABM whose abundance correlations fall in the colored bands identified in (A), suggesting, for example, that the negative correlations in category 1 (gray) are dominated by competition and apparent competition interactions, whereas the strongly positive correlations in category 4 (purple) derive from specialized interactions.

To understand the origins and potential meaning of the four clusters/categories of Gaussians in the empirical data, we used the ABM to simulate the dynamics of hypothetical ecological communities that differed in the importance of prey-predator interactions and competition. We considered trophic-relation-based ABM systems involving prey, specialist predators, and generalist predators, which implicitly also allow for competition and apparent competition (or, intra-guild competition). We compared where the abundance correlations associated with specialist, generalist, and competitive pairwise interactions from the simulated ABM communities fell relative to the four categories obtained via clustering from the fossil correlation distributions. Fully 86% of all correlations derived from interactions in the ABM fell within the intervals of the four empirically defined categories (Figures 2A–2C). In support of our initial ideas about the relationship between abundance correlation and interaction type, we found that ABM interactions involving competition and apparent competition dominate category 1, generalist prey-predator interactions dominate categories 2 and 3, and specialist prey-predator interactions dominate category 4

(Figure 2C). To explore, we used a second ABM in which each prey-predator interaction was weighted by the predator's preference for that prey. From these simulations, we recovered the specialist-generalist spectrum of interactions and further identified a non-linear relation between a predator's preferences for prey and the abundance correlations recovered from the ABM. The abundance correlation between a predator and its lower preference prey was weaker than that expected for the same prey unweighted by preference (Figure S4). In both the ABM models, the final correlations in a wide variety of parameter combinations/conditions exhibited strong effects only from the prey preference (in the second ABM) or from categorization of trophic interactions (in the first ABM where we differentiated specialists from generalists). Other initial conditions and parameters had very small influences on the correlations (see Figure S11)—rendering our results and inferences robust.

With reference to the ABM results, we can interpret that "category 1" (gray) involves negative correlations suggesting competition and apparent competition interactions among taxa (Figure 2C, leftmost column). Alternatively, such negative correlations can also arise if species have different habitat preferences and the relative availability of different habitats changes over time. Similarly, correlations in categories 2 (blue) and 3 (light orange) likely involve generalist consumers. If a consumer is not specializing on one resource but eats many, it will be only loosely correlated with its prey (Figure 2C, middle columns). A weak positive correlation could also mean that both members of a species pair use similar resources. Category 4 (purple) would derive from component Gaussians that feature consistently strong, positive correlations. This category likely represents specialist predation in which a predator depends solely or very strongly on a particular prey species (Figure 2C, rightmost column). Alternatively, if two interacting species are in a mutualistic relationship or exhibit a strong joint dependence on environmental conditions, similarly strong positive correlations could emerge. Please note that throughout our work, we will refer to interactions as specialist or generalist (or competitive) without ascribing roles to particular taxa as we cannot ascertain which species are the prey and the predator in a given pair on the basis of abundance only. Therefore, our network is undirected.

We acknowledge that correlations may exist based on similar habitat/environment and species interactions such as mutualisms that are, unlike the focus of our efforts, neither trophic nor competitive in nature. Indeed, disentangling trophic from non-trophic interactions is overall a more difficult task and would require further paleontological interaction data as well as simulation and analysis work that are beyond the scope of the current analysis.

To look at the effect of habitat, we first calculated the preservation bias for habitat (Figure 1B) and found no significant effect of habitat on the network structure. Next, to support our trophic ABM analysis as a benchmark for categorization, we tested whether two alternative reasons for correlations (i.e., habitat specializations for negative correlations and habitat/environment sharing for positive correlations) impacted our analysis of the fossil data. To do this, we used a stochastic block model (SBM) on the sub-assemblages and on the running time frame data to see if the clustered distributions of interactions could be explained instead by habitat/environment and motility data hypothesized in literature (see Figure S10).

SBMs find community structure in networks (i.e., blocks of nodes which interact more among themselves than with others outside the block) and in this application would indicate clustering of interactions based on similar habitat or motility (Karrer and Newman, 2011). To implement the SBMs, we first computed the Shannon's equitability index of each block in a given network and then calculated the weighted average of this index across blocks. An index value of 1 implies equal distribution of habitat or motility types across blocks, while a 0 indicates complete dominance of one type in a block. The SBM analyses revealed no strong dependence of the empirical correlations on either habitat or motility (Figure S10C).

Lastly, to explore whether negative correlations can arise from species specializing on different habitats, we compared the frequency of negative correlations within the same habitat to the corresponding values for different habitats. For the running timescale data, there were no more negative interactions among taxa from different habitats than from the same habitats (Pearson's X^2 with Yates' continuity correction: mean p value [across the entire running time frame analysis] = 0.89, range = [0.68,0.93]), thereby excluding any strong effect of habitat exclusivity. We found similar results for positive correlations, again finding an absence of association between interactions and species' habitat types (Pearson's X^2 with Yates' continuity correction: mean p value [for all time frame analysis] = 0.26, range = [0.19,0.35]). Collectively, these results suggest that habitat did not play a significant role in the structure, value, and distribution of correlations in

our network and that these correlations instead likely stem from species interactions. Note that in our case, we are assuming that in absence of discernable effects from habitat bias, body type bias, or size bias, the statistically corrected, inferred interactions are either trophic or competitive in nature only. Future data and work are necessary to tease apart other forms of species interactions.

Refocusing on the distributions of correlations, we observe that across fossil sub-assemblages A-D, negative interactions increase in relative frequency over time (Figures 2A and 2B). Similarly, specialist and generalist interactions increased from sub-assemblage A to B, but specialist interactions are largely absent in D and occur only infrequently in C. Systematic change in the fossil transport regime could explain this, but this seems unlikely given the consistency of pairwise correlation signals over time (see Figure S9). Alternatively, long-term environmental change could have decreased regional productivity and made resources rare in the area of fossilization. Such long-term loss of productivity could have led to an increase in competitive interactions and loss of specialist interactions (including both mutualists and trophic interactions), which are more prone to extinctions (or extirpations) (Ryall and Fahrig, 2006; Colles et al., 2009). These results contrast with previous food-web-based studies, where generalists dominate early structuring of food webs, followed by specialists (Piechnik et al., 2008). As such, instead of representing colonization of new habitats, our data set may provide a window into fluctuating ecological abundances transported locally in a near-shore habitat, which were fossilized during intermittent episodes of exceptional preservation. Although we do not know the time frame of deposition of RQ exactly—and it might be fairly long—there are no anatomical changes observable in the fossil taxa, which are consistently present throughout the assemblage. This suggests that the assemblage remains within an ecological regime rather than reflecting evolutionary time.

Analyses of abundance correlation networks recovered many proposed prey-predator interactions. We used the term "consensus interactions" to refer to those species pairs whose abundance correlation yielded the same interaction categorization for a majority of the strata (>50%) where the two taxa co-occurred (see Figure S9 for details). For species whose trophic interactions have been described or suggested in past literature and whose abundance in this data set was sufficient for correlation analysis (Figure 3, innermost region), fully 83.5% (71 of 85) of consensus interactions predicted through our correlational analyses have been independently proposed in paleontological literature (collected from Dunne et al., 2008; Erwin and Valentine, 2012; see methods). Our analyses supplement these expert propositions by assigning pairwise interactions into categories of prey specialization or preference by reference to correlation categories (Figure 2). Furthermore, we propose 117 new possible pairwise trophic interactions based on abundance correlations identified here. These include 75 putative interactions for species whose trophic interactions were previously only partially known (Figure 3, innermost submatrix) and another 42 putative interactions involving species whose trophic interactions were not previously reported. Lastly, 18 pairwise interactions previously known from the literature could not be recovered here because the taxa involved were represented at very low densities in the fossil data set (Figure 3, submatrix with red background).

To put these results into better context, we can take the example of the enigmatic lobopodian *Hallucigenia*, which has been proposed to feed on sponges due to its limb morphology and co-occurrence with the sponge *Vauxia* (see Zhuravlev, 2001; Dunne et al., 2008). In this work, we predict a prey-predator relationship between *Hallucigenia* and *Vauxia*, as well as between *Hallucigenia* and other sponges such as *Choia*, *Takakkawia*, *Hazelia*, and *Hamptonia* (See Figure 3), therefore matching past expectations. The nature of the correlation, based on our model, suggests that *Hallucigenia* might be a generalist feeder on sponges (see Figure S8). In past literature, *Hallucigenia* has been proposed to be eaten by *Oryctocephalus* and *Parkaspis*, due to their hypostome structure, gnathobases, and limb morphology (Fortey and Owens, 1999; Dunne et al., 2008), and we recover both these interactions (Figures 3 and S8). Our model also predicts a relationship between *Hallucigenia* and *Ottoia*, with possibly the latter as a predator/scavenger on the former, as *Ottoia* is also known from fossilized gut contents to feed on epibenthic organisms such as hyoliths (*Haplophrentis*), agnostids, brachiopods (*Micromitra*), trilobites, and arthropods (*Sidneyia*) (see Vannier, 2012), and we recover most of these relationships from our analysis. We also propose that *Hallucigenia* might have been preyed upon by the anomalocaridid *Laggania* but not by other anomalocaridids; this may reflect the unique ecology of *Laggania* or it may be a spurious association due to other factors.

Anomalocaris and other anomalocaridids such as *Laggania* and *Hurdia* are known to be large predators with well-developed appendages, complex digestive systems, large eyes, and active swimming (Briggs et al., 1994; Daley et al., 2013; Vannier et al., 2014). Our model suggests a large repertoire of prey for them, such as

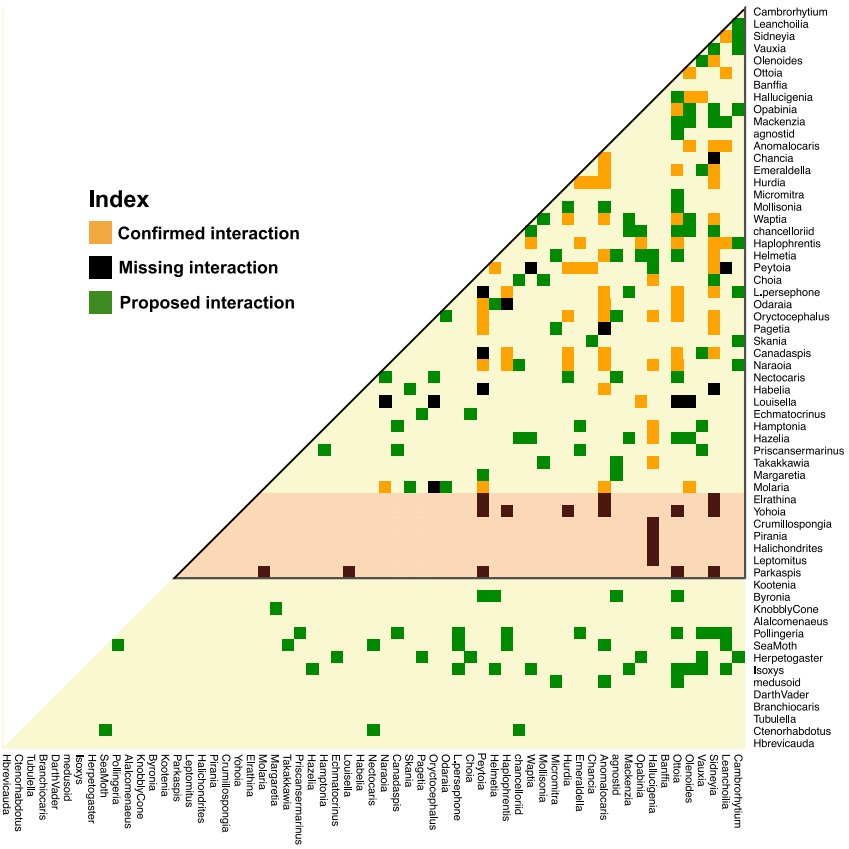

Figure 3. Inferred species interactions

Species interaction half-matrix showing consensus interactions from our analysis, as compared with known trophic interactions from literature (Butterfield., 2003; Dunne et al., 2008; Erwin and Valentine, 2012). Confirmed interactions were proposed in the literature and supported in the correlation analyses here. Missing interactions are reported elsewhere but did not obtain any support from our abundance correlation analyses. Proposed interactions are not currently known from the paleontological literature but are suggested by analyses here. The subset of species interactions inside the black triangle were posited in previous studies (Dunne et al., 2008). The species within the light orange area were numerically rare in our data set and no statistically robust prediction could be made regarding their interactions. For classification of confirmed interactions, see Figure S8, and for consistency of interaction, see Figure S9.

smaller arthropods like *Leanchoilia, Sidneyia, Olenoides, Chancia, Emeraldella, Waptia, and Helmetia* (Figures 3 and S8). The predatory taxa could capture these smaller arthropods using their vision, spiny appendages, and swimming prowess from either nektonic or epibenthic environments. Most of these model predictions are supported by previous literature (see Dunne et al., 2008). Figure 3 outlines many such interactions between various taxa from RQ and discussing them at length would not be feasible in this work. We therefore leave it to the reader to explore the details present in this figure (and its more detailed version, Figure S8).

Results in Figure 3 only considered trophic interactions. Our correlational analyses also identified 137 possible competitive (both direct and indirect) interactions for which there is no reference set because competitive interactions are more difficult to deduce from paleo-biological data (Figure S7). Certain high correlation interactions may have been mutualisms, or based on shared environmental preference, common habitat patterns, or indirect interactions, rather than being trophic in nature (Freilich et al., 2018). We searched, unsuccessfully, for a strong habitat dependence in the fossil data (see Figure S10 and other analyses above) but still cannot rule out any of these alternative possibilities with current data. Direct fossil evidence and further paleontological knowledge is needed to verify or explore these points.

Detailed ecological analyses of correlation networks may suffer from overestimation problems (Carr et al., 2019; Freilich et al., 2018), but broader brush categorization of interactions based on abundance

correlations can provide insights into the functional characteristics of fossil assemblages. Predicted interactions can be supplemented with interactions proposed by paleontological literature, based on gut contents, morphology, or other analyses, to weed out false positives. Other problems raised by earlier studies of paleoecological networks (Dunne et al., 2008; Roopnarine, 2010), such as whether correlations capture long-term prey-predator and population dynamics, were also explored here. We found that abundance correlation analyses echo results concerning long-term correlations in prey-predator models (Carr et al., 2019) and provide a strong platform for predicting species interactions without reference to prior information concerning the incidence, intensity, or character of those interactions (Figures S4 and S5). Due to these reasons, we do not go further in describing the nature and implications of the proposed interactions but rather leave it to further filtering and scrutiny by future paleo-biological studies.

Understanding ecological dynamics from fossil data has always been a major challenge, especially for older assemblages. The extraordinary fossil preservation of the Burgess Shale, including the RQ data set reported here, provides an exceptional window on possible ecological interactions during an era of major animal evolution. Past studies argued that many properties of modern ecosystem structure first emerged during the Cambrian (Bengtson, 2002), and network analyses coupled with proposed trophic interactions highlighted aspects of food web structure during this period (Dunne et al., 2008). When sufficiently strong fossil data are available, analyses of abundance correlation networks, supplemented with models to characterize biases in preservation and interpret species interactions, as outlined in our work, can reveal unknown or difficult-to-ascertain links in fossilized ecosystems and shed light on trophodynamics over evolutionary time.

Limitations of the study

The major limitation of our approach is that biases that involve ecological or behavioral aspects of species interactions that are not expressed through a biased representation in habitat type, body type, or body size cannot be disentangled from trophic and competitive interactions. Mutualisms in particular remain unaddressed following this work. Further modeling and analysis work as well as paleontological interaction data are needed to validate or invalidate the inferences from our analysis.

Resource availability

Lead contact

Further information and requests for resources should be directed to and will be fulfilled by the lead contact, Anshuman Swain (answain@terpmail.umd.edu)

Material availability

Not applicable.

Data and code availability

All relevant data needed to recreate the results are provided as supplementary material. Abundance values for all the taxa at 10 cm resolution in RQ can be found as 'abundance.csv' in Data S1; ecological habits, taxonomic affinity, body type categorization, and size metadata for all the taxa can be found as 'metadata_traits.csv' in Data S1. Relevant final data are also provided for reference—'Trophic interaction_matrix.csv' in Data S1 contains the consensus trophic interactions, and competitive_interaction_matrix' in Data S1 contains the consensus competitive/negative interactions. Simplified ABM simulation and network analysis code (along with the data) can be found at: github.com/anshuman21111/cambrian-fossil-networks.

METHODS

All methods can be found in the accompanying transparent methods supplemental file.

SUPPLEMENTAL INFORMATION

Supplemental information can be found online at https://doi.org/10.1016/j.isci.2021.102271.

ACKNOWLEDGMENTS

We thank Nicholas J Butterfield, Phillip Staniczenko, Jennifer Dunne, Michelle Girvan, Hector Corrada-Bravo, Tracy Chen, Sushant Patkar, Roozbeh Bassirian, Doug Erwin, Philip Johnson, and Jake Weissman for their helpful

suggestions and discussions. We acknowledge help from Jack O Shaw in collecting some of the metadata for our analysis. A.S.'s contribution to this research was supported in part by training through NSF award DGE-1632976. We would also like to acknowledge the Royal Ontario Museum (Toronto, ON, Canada) online database on Cambrian organisms, which provides stratigraphic occurrence, updated taxonomy, palaeoecology, and accurate anatomical reconstructions for taxa discussed in this study.

AUTHOR CONTRIBUTIONS

Conceptualization, A.S. and W.F.F.; methodology, A.S., M.D., and W.F.F.; investigation, A.S., M.D., and W.F.F.; writing – original draft, A.S. and W.F.F.; writing – review & editing, A.S., M.D., and W.F.F; resources, M.D. and A.S.; project administration, W.F.F. and A.S.; formal analysis, software and visualization: A.S.; data curation: A.S. and M.D.

DECLARATION OF INTERESTS

The authors declare no competing interests.

INCLUSION AND DIVERSITY

One or more of the authors of this paper self-identifies as an underrepresented ethnic minority in science. While citing references scientifically relevant for this work, we also actively worked to promote gender balance in our reference list.

Received: September 23, 2020
Revised: December 7, 2020
Accepted: March 2, 2021
Published: April 23, 2021

REFERENCES

Armitage, D.W., and Jones, S.E. (2019). How sample heterogeneity can obscure the signal of microbial interactions. ISME J. *13*, 2639–2646.

Barberán, A., Bates, S.T., Casamayor, E.O., and Fierer, N. (2012). Using network analysis to explore co-occurrence patterns in soil microbial communities. ISME J. *6*, 343.

Bengtson, S. (2002). Origins and early evolution of predation. Paleontolog. Soc. Pap. *8*, 289–318.

Blasius, B., Rudolf, L., Weithoff, G., Gaedke, U., and Fussmann, G.F. (2020). Long-term cyclic persistence in an experimental predator–prey system. Nature *577*, 226–230.

Briggs, D.E., Collier, F.J., and Erwin, D.H. (1994). The fossils of the Burgess Shale (No. 562 BRI).

Butterfield, N.J. (2003). Exceptional fossil preservation and the Cambrian explosion. Integr. Comp. Biol. *43*, 166–177.

Buzas, M.A., and Hayek, L.A.C. (1998). SHE analysis for biofacies identification. J. Foraminiferal Res. *28*, 233–239.

Carbone, C., and Narbonne, G.M. (2014). When life got smart: the evolution of behavioral complexity through the ediacaran and early cambrian of NW Canada. J. Paleontol. *88*, 309–330.

Carr, A., Diener, C., Baliga, N.S., and Gibbons, S.M. (2019). Use and abuse of correlation analyses in microbial ecology. ISME J. *13*, 2647–2655.

Clarke, K.R., and Warwick, R.M. (1994). Similarity-based testing for community pattern: the two-way layout with no replication. Mar. Biol. *118*, 167–176.

Caron, J.B., and Jackson, D.A. (2006). Taphonomy of the greater phyllopod bed community, Burgess Shale. Palaios *21*, 451–465.

Caron, J.B., and Jackson, D.A. (2008). Paleoecology of the greater phyllopod bed community, Burgess Shale. Palaeogeogr. Palaeoclimatol. Palaeoecol. *258*, 222–256.

Colles, A., Liow, L.H., and Prinzing, A. (2009). Are specialists at risk under environmental change? Neoecological, paleoecological and phylogenetic approaches. Ecol. Lett. *12*, 849–863.

Daley, A.C., Budd, G.E., and Caron, J.B. (2013). Morphology and systematics of the anomalocaridid arthropod Hurdia from the middle cambrian of British Columbia and Utah. J. Syst. Palaeontol. *11*, 743–787.

Delmas, E., Besson, M., Brice, M.H., Burkle, L.A., Dalla Riva, G.V., Fortin, M.J., Gravel, D., Guimarães, P.R., Jr., Hembry, D.H., Newman, E.A., and Olesen, J.M. (2017). Analysing ecological networks of species interactions. Biol. Rev.

Devereux, M.G. (2001). Palaeoecology of the Middle Cambrian Raymond Quarry Fauna (Burgess Shale).

Dormann, C.F., Fründ, J., and Schaefer, H.M. (2017). Identifying causes of patterns in ecological networks: opportunities and limitations. Annu. Rev. Ecol. Evol. Syst. *48*, 559–584.

Dunne, J.A., Williams, R.J., Martinez, N.D., Wood, R.A., and Erwin, D.H. (2008). Compilation and network analyses of Cambrian food webs. PLoS Biol. *6*, e102.

Erwin, D.H., Laflamme, M., Tweedt, S.M., Sperling, E.A., Pisani, D., and Peterson, K.J. (2011). The Cambrian conundrum: early divergence and later ecological success in the early history of animals. Science *334*, 1091–1097.

Erwin, D.H., and Valentine, J.W. (2012). The Cambrian Explosion: The Construction of Animal Biodiversity (Roberts).

Flannery Sutherland, J.T., Moon, B.C., Stubbs, T.L., and Benton, M.J. (2019). Does exceptional preservation distort our view of disparity in the fossil record? Proc. R. Soc. B *286*, 20190091.

Fortey, R.A., and Owens, R.M. (1999). Feeding habits in trilobites. Palaeontology *42*, 429–465.

Freilich, M.A., Wieters, E., Broitman, B.R., Marquet, P.A., and Navarrete, S.A. (2018). Species co-occurrence networks: can they reveal trophic and non-trophic interactions in ecological communities? Ecology *99*, 690–699.

Gaines, R.R., Hammarlund, E.U., Hou, X., Qi, C., Gabbott, S.E., Zhao, Y., Peng, J., and Canfield, D.E. (2012). Mechanism for burgess shale-type preservation. Proc. Natl. Acad. Sci. U S A *109*, 5180–5184.

Ings, T.C., Montoya, J.M., Bascompte, J., Blüthgen, N., Brown, L., Dormann, C.F., Edwards, F., Figueroa, D., Jacob, U., Jones, J.I., and Lauridsen, R.B. (2009). Ecological networks–beyond food webs. J. Anim. Ecol. *78*, 253–269.

Jordano, P. (2016). Sampling networks of ecological interactions. Funct. Ecol. *30*, 1883–1893.

Karrer, B., and Newman, M.E. (2011). Stochastic blockmodels and community structure in networks. Phys. Rev. E *83*, 016107.

Kidwell, S.M., Bosence, D.W., Allison, P.A., and Briggs, D.E.G. (1991). Taphonomy and time-averaging of marine shelly faunas. Taphonomy: Releasing the Data Locked in the Fossil Record (Plenum), pp. 115–209.

Kidwell, S.M. (2001). Preservation of species abundance in marine death assemblages. Science *294*, 1091–1094.

Koch, C.F. (1978). Bias in the published fossil record. Paleobiology *4*, 367–372.

Kowalewski, M., Wood, S.L.B., Kiessling, W., Aberhan, M., Fürsich, F.T., Scarponi, D., and Hoffmeister, A.P. (2006). Ecological, taxonomic, and taphonomic components of the post-Paleozoic increase in sample-level species diversity of marine benthos. Paleobiology *32*, 533–561.

Lee, M.S., Soubrier, J., and Gregory, D. (2013). Edgecombe. Rates of phenotypic and genomic evolution during the Cambrian explosion. Curr. Biol. *23*, 1889–1895.

Liebhold, A., Koenig, W.D., and Bjørnstad, O.N. (2004). Spatial synchrony in population dynamics. Annu. Rev. Ecol. Evol. Syst. *35*, 467–490.

Mángano, M.G., and Buatois, L.A. (2014). Decoupling of body-plan diversification and ecological structuring during the Ediacaran–Cambrian transition: evolutionary and geobiological feedbacks. Proc. R. Soc. B: Biol. Sci. *281*, 20140038.

Martin, R.E. (1999). Taphonomy: A Process Approach, *Vol. 4* (Cambridge University Press).

Mitchell, E.G., Harris, S., Kenchington, C.G., Vixseboxse, P., Roberts, L., Clark, C., Dennis, A., Liu, A.G., and Wilby, P.R. (2019). The importance of neutral over niche processes in structuring Ediacaran early animal communities. Ecol. Lett. *22*, 2028–2038.

Mitchell, E.G., and Butterfield, N.J. (2018). Spatial analyses of ediacaran communities at mistaken point". Paleobiology *44*, 40–57.

Mitchell, J.S. (2015). Preservation is predictable: quantifying the effect of taphonomic biases on ecological disparity in birds. Paleobiology *41*, 353–367.

Morris, S.C. (1986). The community structure of the Middle Cambrian phyllopod bed (Burgess Shale). Palaeontology *29*, 423–467.

Muscente, A.D., Bykova, N., Boag, T.H., Buatois, L.A., Mángano, M.G., Eleish, A., Prabhu, A., Pan, F., Meyer, M.B., Schiffbauer, J.D., and Fox, P. (2019). Ediacaran biozones identified with network analysis provide evidence for pulsed extinctions of early complex life. Nat. Commun. *10*, 1–15.

Muscente, A.D., Prabhu, A., Zhong, H., Eleish, A., Meyer, M.B., Fox, P., Hazen, R.M., and Knoll, A.H. (2018). Quantifying ecological impacts of mass extinctions with network analysis of fossil communities. Proc. Natl. Acad. Sci. U S A *115*, 5217–5222.

Olson, E.C., Behrensmeyer, A.K. and Hill, A.P. (1980). Taphonomy: Its History and Role in Community Evolution. Fossils in the Making: Vertebrate Taphonomy and Paleoecology, 5-19. https://books.google.com/books?hl=en&lr=&id=a44hwSFpdpgC&oi=fnd&pg=PA5&dq=Olson,+E.C.,+Behrensmeyer,+A.K.+and+Hill,+A.P.+(1980).+Taphonomy:+Its+History+and+Role+in+Community+Evolution.+Fossils+in+the+Making:+Vertebrate+Taphonomy+and+Paleoecology,+5-19.&ots=k-cc5e8zeh&sig=mDUPQVuZWtdfwtQ803UwbQ-oX6w#v=onepage&q&f=false

Orr, P.J., Benton, M.J., and Briggs, D.E. (2003). Post-Cambrian closure of the deep-water slope-basin taphonomic window. Geology *31*, 769–772.

Piechnik, D.A., Lawler, S.P., and Martinez, N.D. (2008). Food-web assembly during a classic biogeographic study: species'"trophic breadth" corresponds to colonization order. Oikos *117*, 665–674.

Poisot, T., Stouffer, D.B., and Kefi, S. (2016). Describe, understand and predict: why do we need networks in ecology? Funct. Ecol. *30*, 1878–1882.

Robins, G., Pattison, P., and Woolcock, J. (2004). Missing data in networks: exponential random graph (p*) models for networks with non-respondents. Soc. Netw. *26*, 257–283.

Roopnarine, P.D. (2010). Networks, extinction and paleocommunity food webs. Paleontol. Soc. Pap. *16*, 143–161.

Ryall, K.L., and Fahrig, L. (2006). Response of predators to loss and fragmentation of prey habitat: a review of theory. Ecology *87*, 1086–1093.

Saleh, F., Antcliffe, J.B., Lefebvre, B., Pittet, B., Laibl, L., Peris, F.P., Lustri, L., Gueriau, P., and Daley, A.C. (2020). Taphonomic bias in exceptionally preserved biotas. Earth Planet. Sci. Lett. *529*, 115873.

Schiffbauer, J.D., Xiao, S., Cai, Y., Wallace, A.F., Hua, H., Hunter, J.,., and Kaufman, A.J. (2014). A unifying model for Neoproterozoic–Palaeozoic exceptional fossil preservation through pyritization and carbonaceous compression. Nat. Commun. *5*, 1–12.

Seilacher, A., Buatois, L.A., and Mángano, M.G. (2005). Trace fossils in the Ediacaran–Cambrian transition: behavioral diversification, ecological turnover and environmental shift. Palaeogeogr. Palaeoclimatol. Palaeoecol. *227*, 323–356.

Shaw, J.O., Coco, E., Wootton, K., Daems, D., Gillreath-Brown, A., Swain, A., and Dunne, J.A. (2021). Disentangling Ecological and Taphonomic Signals in Ancient Food webs. Paleobiology (Cambridge University Press), pp. 1–17, https://doi.org/10.1017/pab.2020.59.

Smith, A.B. (2001). Large–scale heterogeneity of the fossil record: implications for Phanerozoic biodiversity studies. Philos. Trans. R. Soc. Lond. Ser. B Biol. Sci. *356*, 351–367.

Sperling, E.A., Balthasar, U., and Skovsted, C.B. (2018). On the edge of exceptional preservation: insights into the role of redox state in Burgess Shale-type taphonomic windows from the Mural Formation, Alberta, Canada. Emerging Top. Life Sci. *2*, 311–323.

Starrfelt, J., and Liow, L.H. (2016). How many dinosaur species were there? Fossil bias and true richness estimated using a Poisson sampling model. Philos. Trans. R. Soc. B: Biol. Sci. *371*, 20150219.

Tobin, P.C., and Bjørnstad, O.N. (2003). Spatial dynamics and cross-correlation in a transient predator–prey system. J. Anim. Ecol. *72*, 460–467.

Tibshirani, R., Walther, G., and Hastie, T. (2001). Estimating the number of clusters in a data set via the gap statistic. J. R. Stat. Soc. Ser. B (Stat. Methodol.) *63*, 411–423.

Vannier, J., and Chen, J. (2005). Early Cambrian food chain: new evidence from fossil aggregates in the Maotianshan Shale biota, SW China. Palaios *20*, 3–26.

Vannier, J., Liu, J., Lerosey-Aubril, R., Vinther, J., and Daley, A.C. (2014). Sophisticated digestive systems in early arthropods. Nat. Commun. *5*, 1–9.

Vannier, J. (2012). Gut contents as direct indicators for trophic relationships in the Cambrian marine ecosystem. PLoS One *7*, e52200.

Zhang, W. (2011). Constructing ecological interaction networks by correlation analysis: hints from community sampling. Netw. Biol. *1*, 81.

Zhao, F., Caron, J.B., Bottjer, D.J., Hu, S., Yin, Z., and Zhu, M. (2014). Diversity and species abundance patterns of the early cambrian (series 2, stage 3) chengjiang biota from China. Paleobiology *40*, 50–69.

Zhuravlev, A.I. (2001). The Ecology of the Cambrian Radiation (Columbia University Press).

iScience, Volume *24*

Supplemental information

Deciphering trophic interactions in a mid-Cambrian assemblage

Anshuman Swain, Matthew Devereux, and William F. Fagan

Supplementary Materials

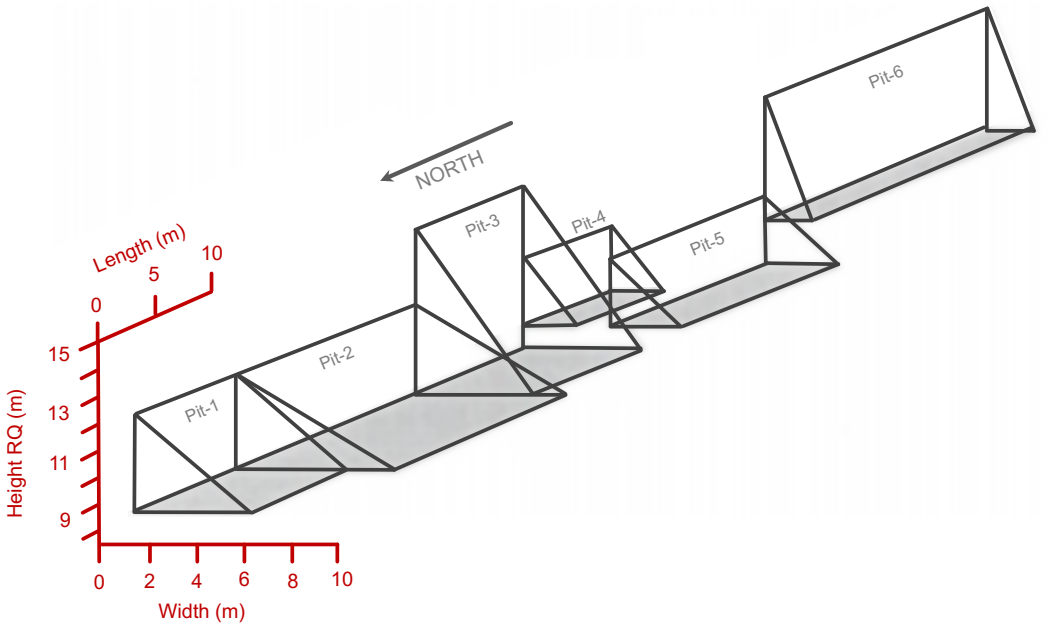

Figure S1: Raymond Quarry Excavation Schematic, related to Figure 1
Schematic of excavations in the Raymond Quarry Member. The original Raymond Quarry was located within Pit #5. The northernmost extent of Pit # l is 23 m south of the Cathedral Escarpment.

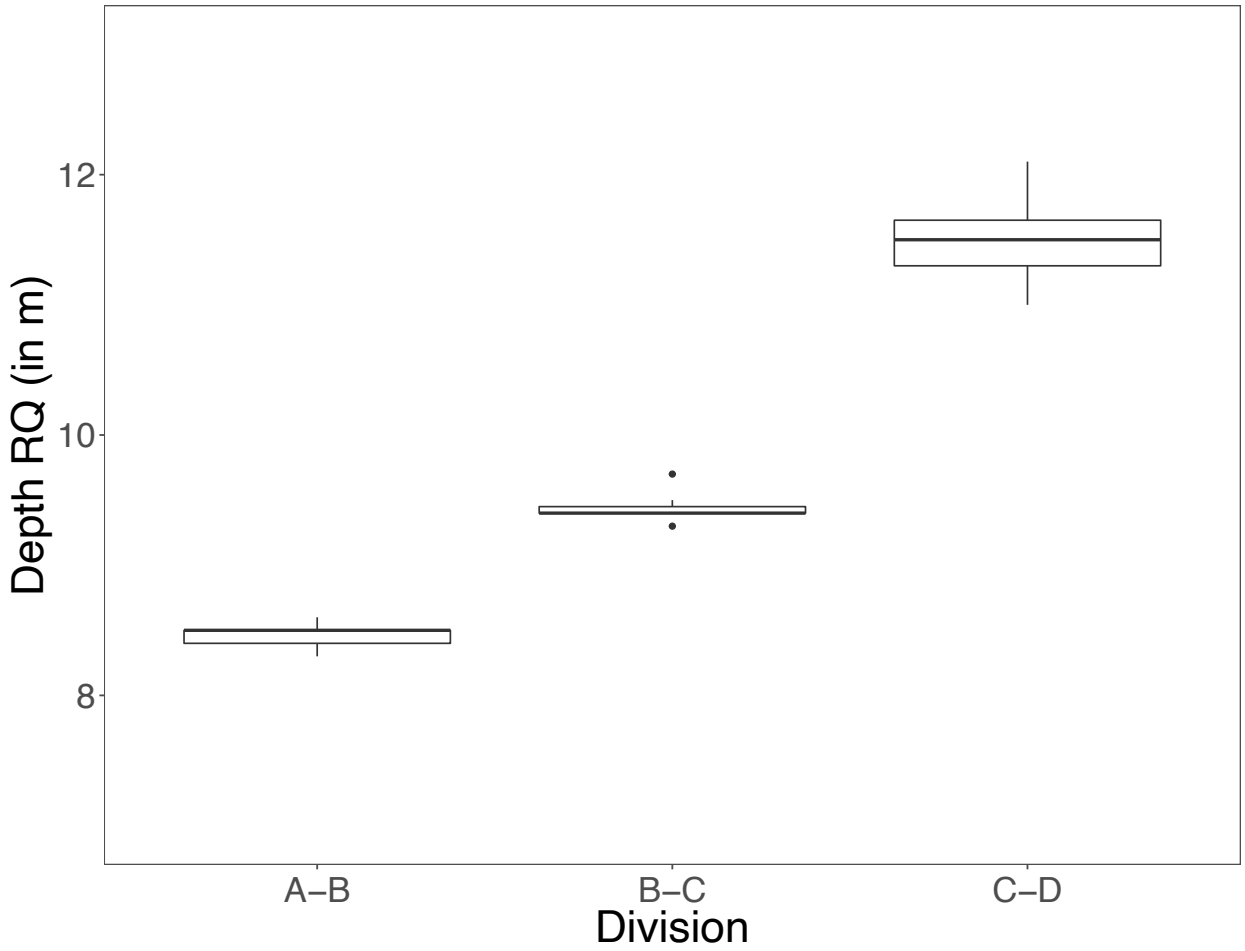

Figure S2: Biofacies detection, related to Figure 1
Biofacies detected using consensus of statistical methods ANOSIM and SHEBI for the boundaries between the Raymond Quarry sub-assemblages A-B, B-C, and C-D.

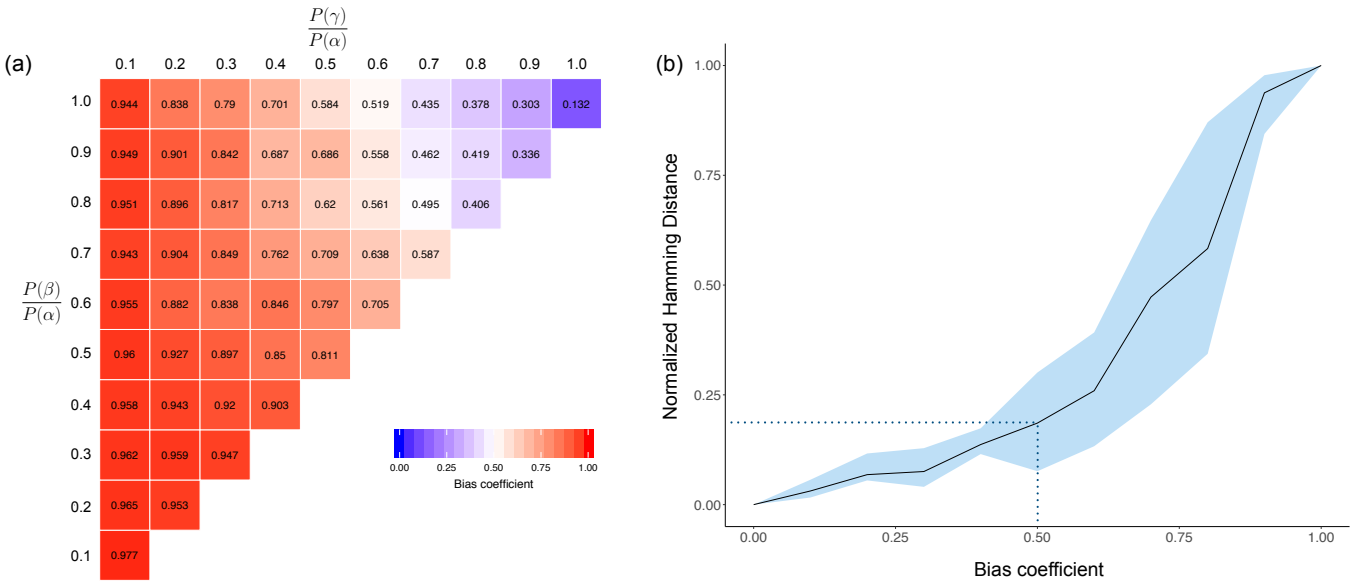

Figure S3: Preservation Bias, related to Figure 1
(a) Plot of bias coefficient as measured from the agent-based model for three categories of preservation probability: α, β and γ; (b) Differences between networks quantified using the Hamming distance (larger values imply greater deviation) as a function of the bias coefficient. The plot compares unaltered ABM networks with ABM networks whose structure was obscured by preservation biases; standard errors are calculated across alternative ABM simulations. Note the nonlinear dependence of Hamming distance on bias that increases steeply beyond bias coefficient of ~0.50.

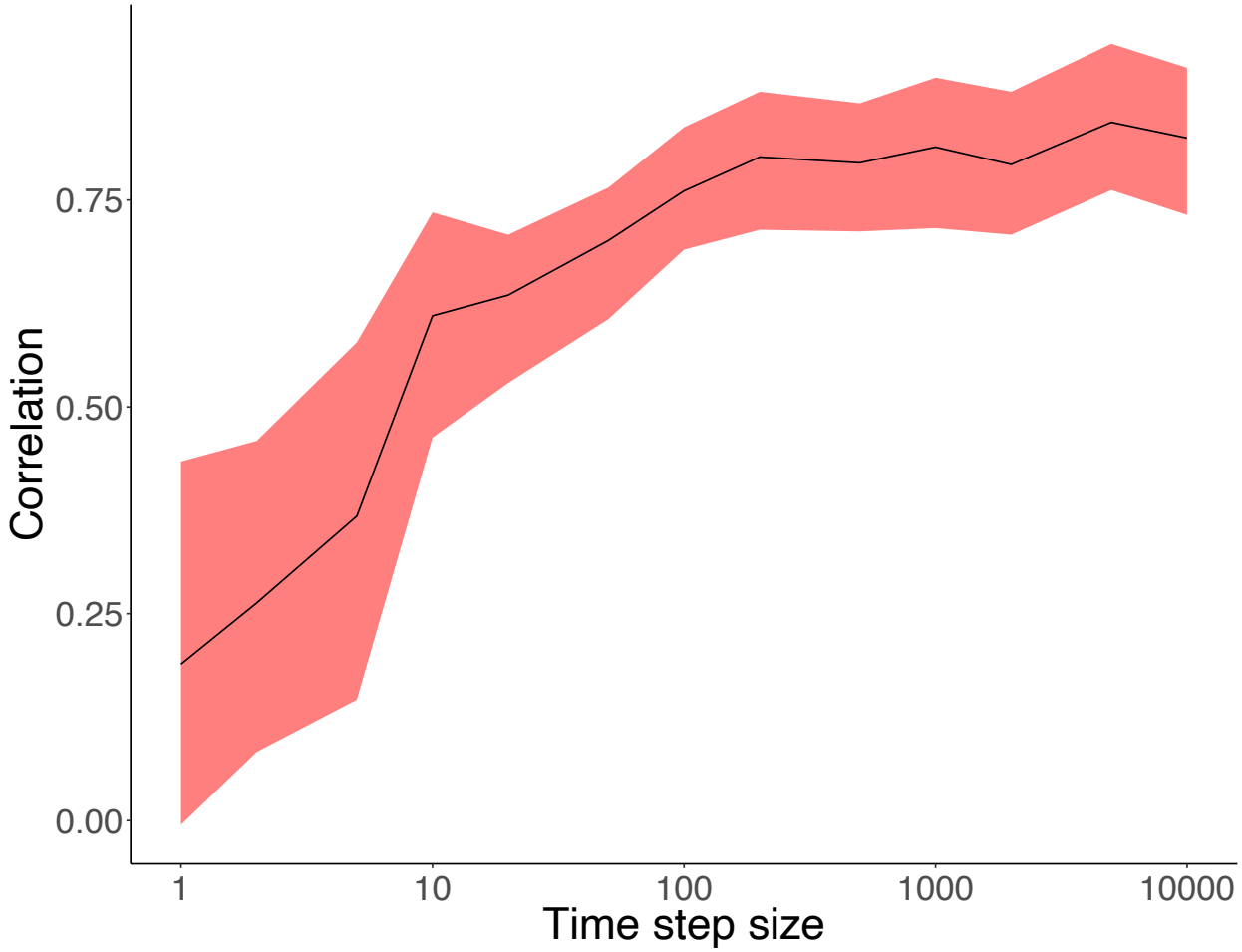

Figure S4: ABM prey-predator correlation, related to Figure 2
Correlation between a prey and its specialist predator in ABM output based on 10 sampled population sizes separated by the specified time steps. The cloud of standard error values was calculated using all the ABM runs with different initial conditions. Each ABM simulation was taken as a separate dataset and the correlation was calculated for each pair of prey and specialist predators in all the datasets. Increasing the number of sampled counts used to calculate the correlation substantially decreases the width of the error cloud.

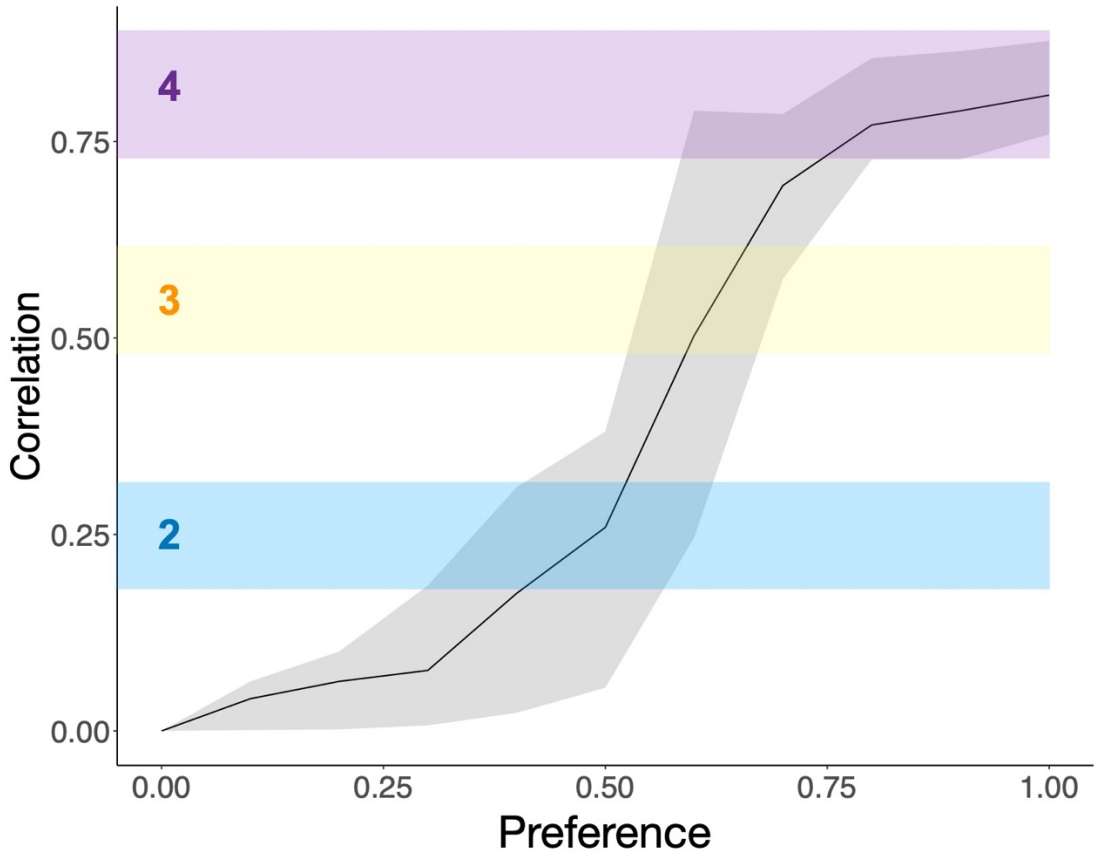

Figure S5: ABM Prey preference correlation, related to Figure 2
Correlation and preference/affinity for prey in an ABM with standard error (run for 10,000 different ABM scenarios). Mapped onto the correlation axis are the three trophic interaction categories 2, 3, and 4 from the spectral analysis.

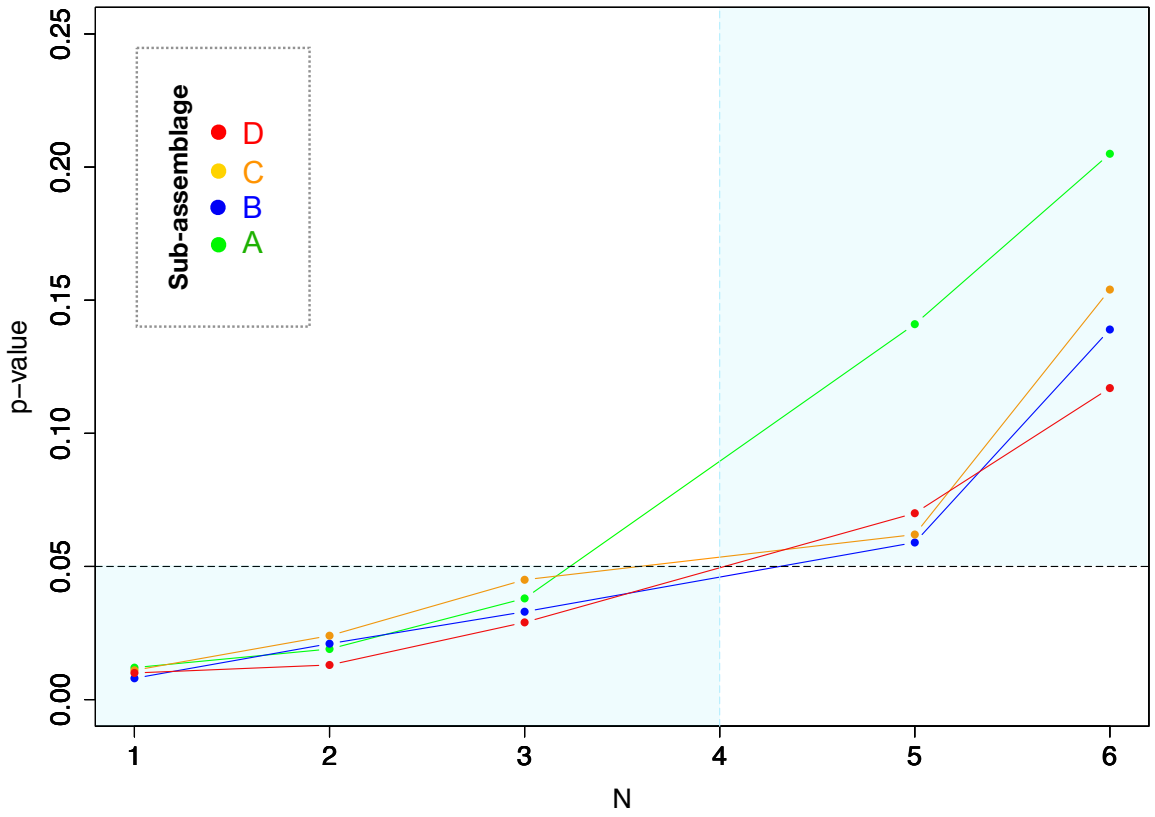

Figure S6: Optimal Clustering, related to Figure 2
p-values from chi-square test of likelihood ratio tests for nested models that differ in the number of Gaussians (N) as compared with a model with 4 Gaussians (for sub-assemblages A-D). The areas highlighted in light blue signify where the model with four Gaussians performs significantly better. All the points for all sub-assemblages lie in the region implying that a model with four basis Gaussians is the best model to pick.

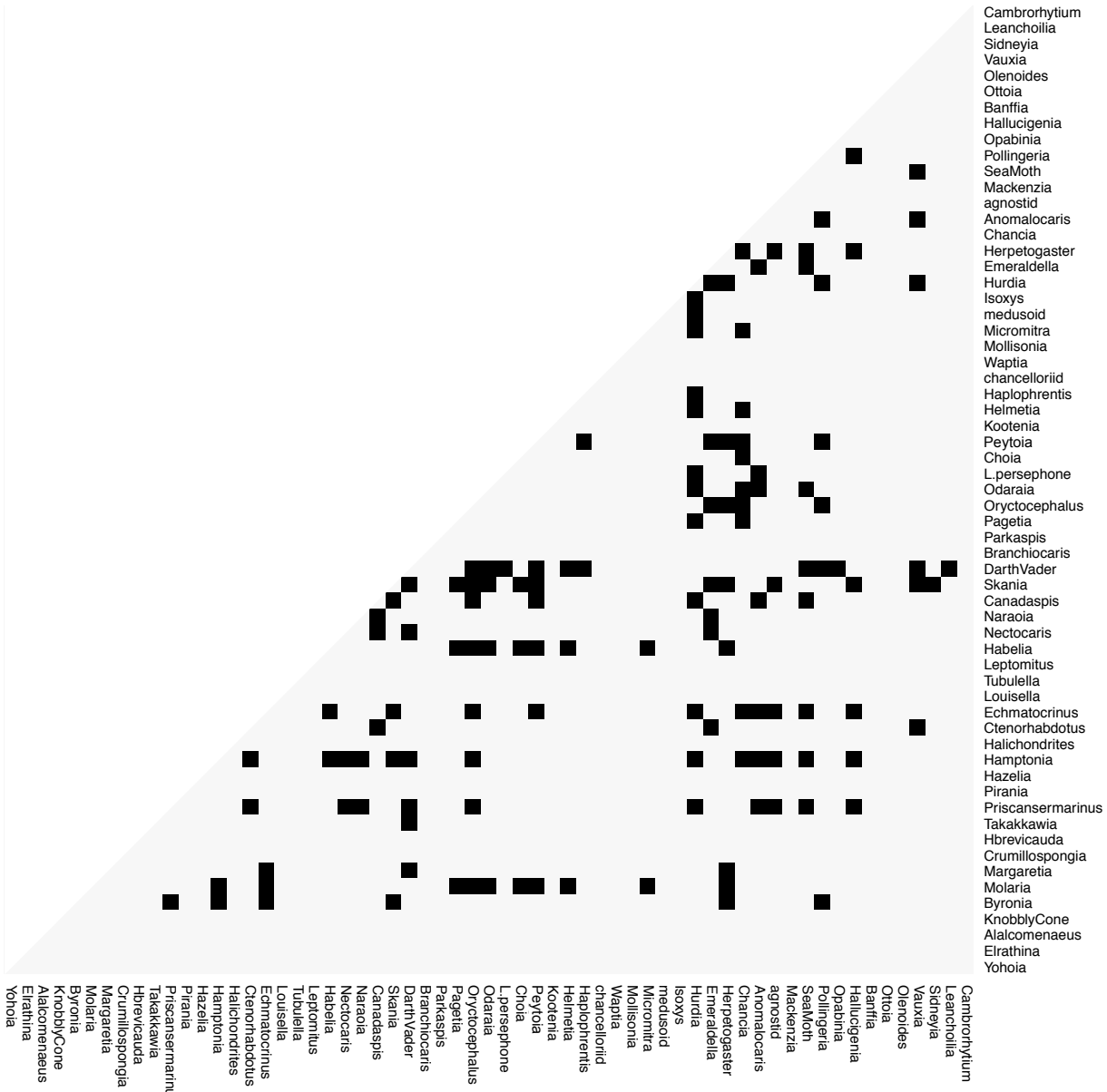

Figure S7: Competitive interactions, related to figure 2
Species interaction half-matrix representing competitive interactions among the fossil taxa proposed on the basis of abundance correlation network analyses. As it is more difficult to test competitive interactions through anatomical or other paleo-ecological evidence, we did not pursue these further, and instead focused only on trophic interactions.

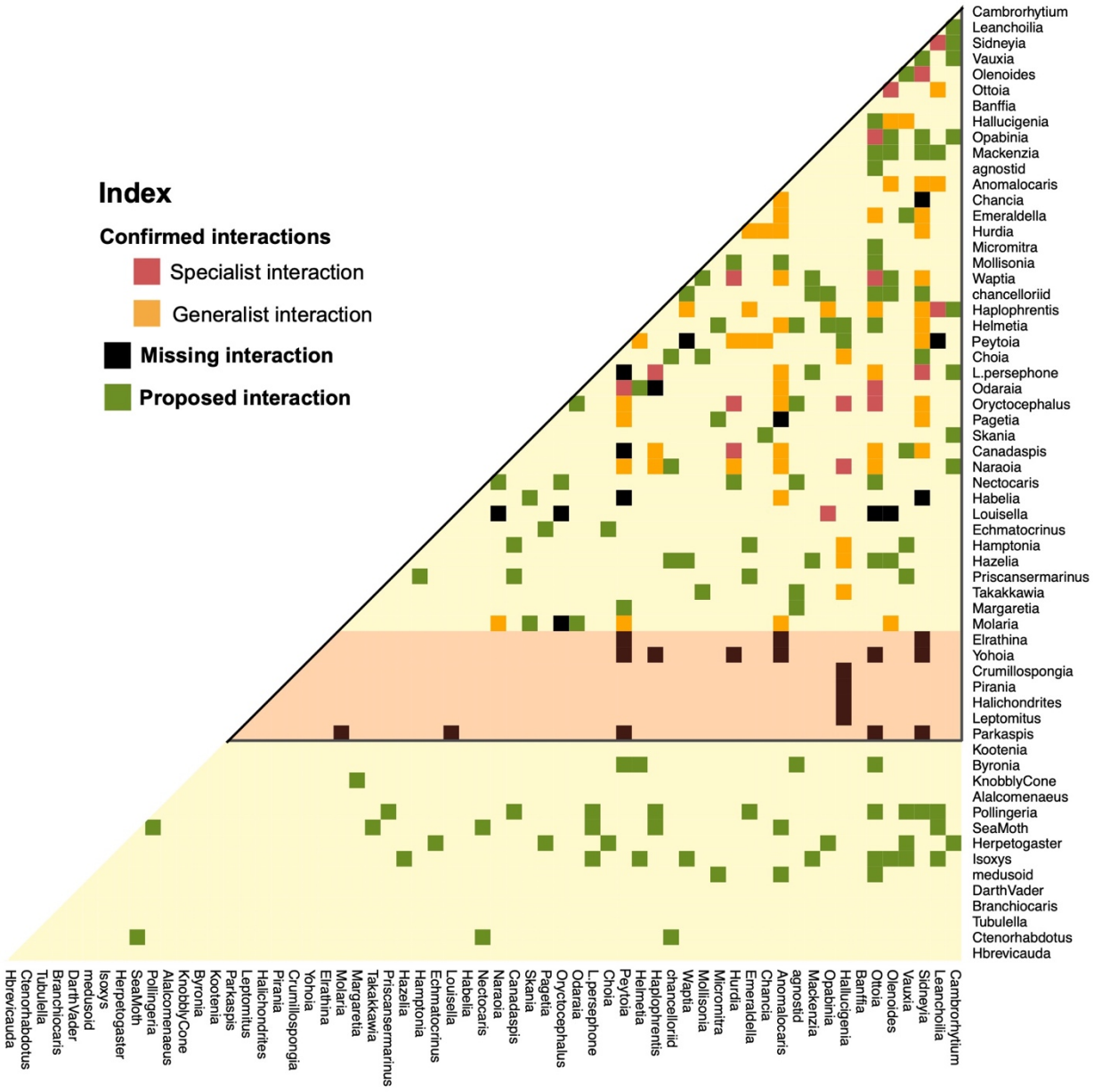

Figure S8: Detailed trophic interaction matrix, related to Figure 2 and Figure 3
Species interaction matrix showing the results from the categorization analysis, as compared with known trophic interactions from literature (Butterfield., 2000; Dunne et al., 2008; Erwin and Valentine, 2013), along with breakdown of the confirmed trophic interactions into specialist and generalist categories. Confirmed interactions were proposed in the literature and supported in the correlation analyses here. Missing interactions are reported elsewhere but did not obtain any support from our abundance correlation analyses. Proposed interactions are not currently known from the paleontological literature but are suggested by analyses here. The subset of species interactions within the black triangle are known from previous studies (Dunne et al., 2008). The species within the light orange area were numerically rare in our dataset and no statistically robust prediction could be made regarding their interactions.

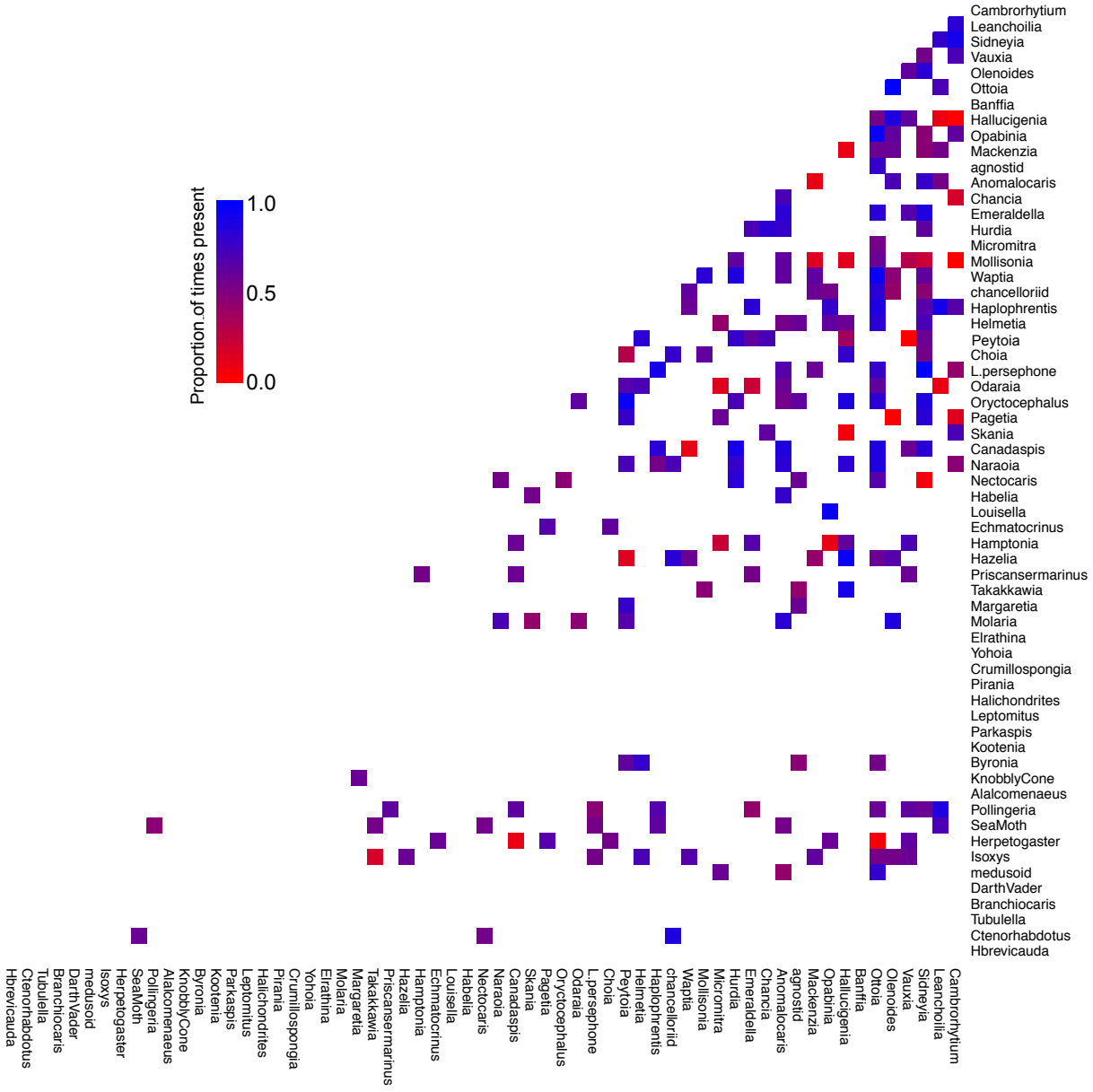

Figure S9: Interaction fidelity, related to Figure 2 and Figure 3
Heatmap showing the proportion of times high fidelity interactions were observed in the same categorization. 82.37% of the high-fidelity interactions are present consistently in the same interaction category more than 50% of the time (of co-occurrences of the pair of species) and are termed as consensus interactions. These consensus interactions are presented in the species interaction half-matrix in figure 3 and S8.

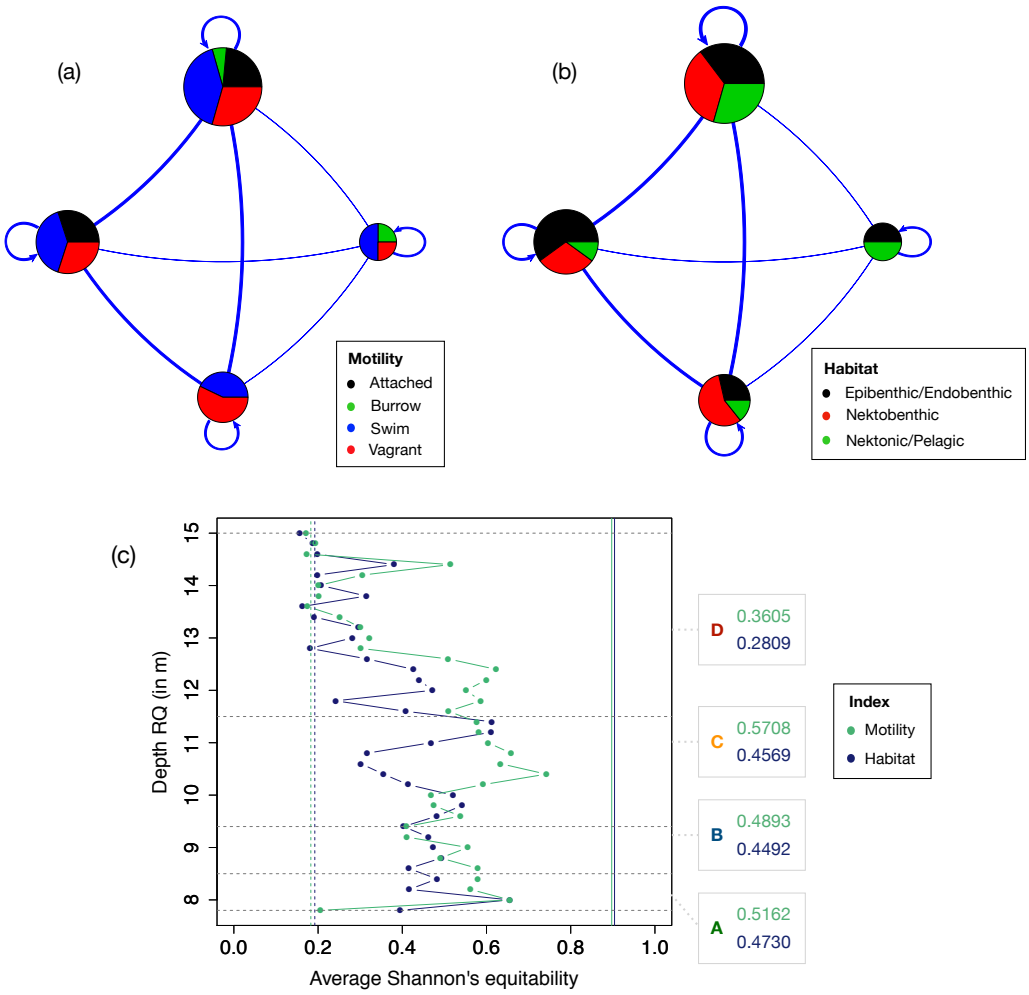

Figure S10: Stochastic block model analysis, related to Figure 1, and Figure 2
A stochastic block model of the overall network (sub-assemblages A-D) is shown here for representation purposes, which depicts four distinct blocks of taxa, estimated using integrated classification likelihood, that interact more within blocks than across blocks for motility classes (a) and habitat affinity classes (b). The lines between groups and their width denotes interaction between two blocks of taxa. Please note that the width of the self-loop here is not meaningful, other than the fact that the taxa within a block interact among themselves. The size of the block refers to the number of taxa in that block. The model has been overlaid here with (a) motility data, and (b) habitat data. Clearly, organisms belonging to particular motility or habitat classes do not fall consistently into SBM blocks. This, in turn, suggests that habitat/motility similarity does not transform into very strong associations through correlations. Please note that the number of blocks varied in different sub-assemblages and running time series analysis, as it is dependent on the structure of the network.
In (c) we use this SBM model to estimate average Shannon's equitability index (SEI) (methods) for the running timeframe analysis and for sub-assemblages (A-D). The grey horizontal dotted lines demarcate the sub-assemblages (A-D). The solid lines (separate for motility and habitat) depict the maximum theoretical value of SEI possible using our data and the dashed lines represent a theoretical SEI for 95% dominance by a single type of habitat/motility (Methods). One can see that, the SEI values depict no dependence of correlation network community structure on habitat or motility, except the start and end of the assemblage – where a weak dependence cannot be ruled out. This is in lines with the bias coefficient (methods, Figure 1(b)).

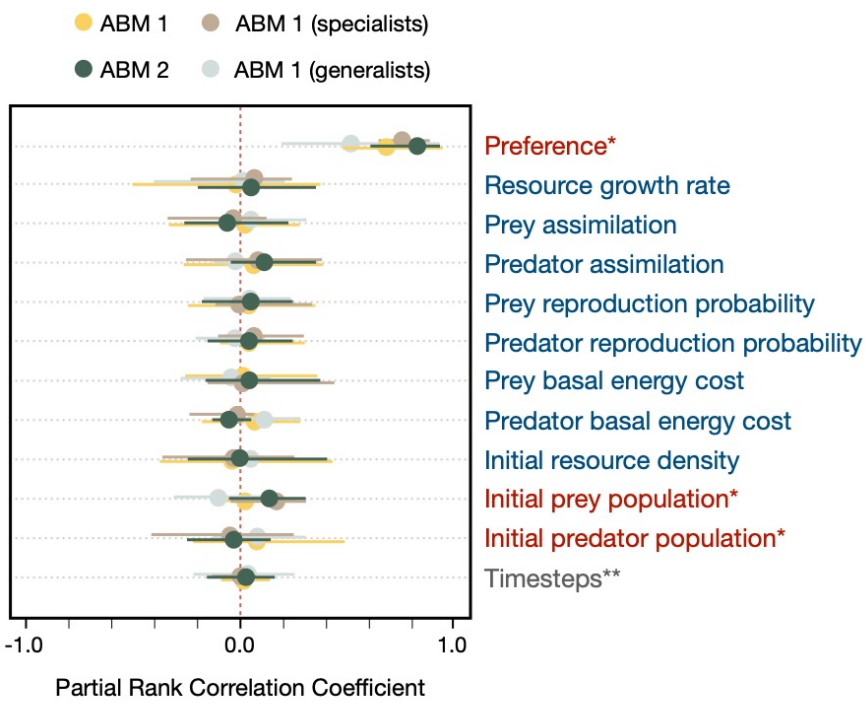

Figure S11: ABM sensitivity analysis, related to Figure 2 and Figure 3
Partial rank correlation coefficient (PRCC) of various initial conditions and parameters for the pairwise predator-prey correlations obtained in the two ABM models. Recall that ABM 1 has specialists and generalists whereas ABM 2 has a random pairwise affinity selection between prey and predators, see methods. Additional results are provided for generalists and specialists in ABM 1. The parameters/initial conditions in red are specific to a given pair of species, and the ones in blue are global parameters or initial conditions. We also examined the effect of timesteps again (see also figure S4). All parameters except resource growth rate, and basal energy costs (for prey and predator) varied between 0 and 1. Resource growth rate varied between 0 and 10, basal energy rates varied between 0.1 and 10 units. Each resource had an energy content of 1 unit. Please note that preference in case of ABM 1 was 1 for specialist interactions and 1/17 for generalist ones (as there were 17 prey species). We used a logistic transform function for PRCC categorization. The initial conditions included prey and predator populations as well as initial resource density – the last one varied between 0 and 1 (as a fraction of total area of the grid). The former two varied between 0 and 20 each. For more details, please refer to the code in the Data availability section.

We used Latin hypercube sampling (LHS) to select the parameters and initial conditions. The error bars represent 95% confidence intervals. This figure tells us that the final correlations in a wide variety of conditions were only strongly affected by the preference/categorization of interactions and were only very weakly affected by other initial conditions or parameters.

Transparent Methods

Data Collection

The primary data were collected from the Raymond Quarry in the main Burgess Shale site (Figure S1), located ~5 km north of Field, British Columbia, Canada, on a ridge connecting Mt. Field and Wapta Mountain ('Fossil Ridge') (figure S1, S2). Other exposures are known, including outcrops on Mt. Stephen that are lithologically and biostratigraphically equivalent to the Raymond Quarry Member (Fletcher and Collins 1998), such as the outcrops of equivalent strata and fossils across the Kicking Horse Valley on the shoulder of Mt. Stephen (Fletcher and Collins 1998). Consequently, the discussed fauna was not geographically isolated. Moreover, and significantly, sediment and fossil evidence support an autochthonous Raymond Quarry fauna.

Vertical bedding measurements were determined from an arbitrarily assigned RQ 10.0 m level (confirmed to be equivalent to 21.6 m above the base of C.D. Walcott's excavations in the Phyllopod Bed). This datum was traceable as a darker weathering bed across the entire exposure of the Raymond Quarry Member, except within approximately 10m of the contact with the Cathedral Escarpment, where fossils become sparse and no material was collected. Beds were subsequently measured vertically and labelled and re-labelled using a permanent marker as blocks were extracted. The first 10m mark was placed in the original Raymond quarry, carved into the rock for permanency between collecting seasons. All fossils were labelled immediately upon discovery according to the bed of occurrence, to the nearest 10cm. Specimens that occurred exactly between two measured levels were assigned to the higher level.

The majority of the physical work utilized hand-tools; no explosives were used. All the bedding planes were thoroughly and uniformly investigated. Despite the comprehensive search, adverse conditions might have rendered some fossils invisible in the field and their numbers cannot be determined exactly, but the effect would have been the same for most organisms and would have approximated their proportions recovered under more favorable conditions. For example, some *Marpolia*-like algal remains may have escaped notice, as they were usually visible only on weathered slabs (often excavated in the previous year). There is some under-representation of the macro-algal component of the community, but it was clearly always a minor contributor. As with any paleontological site, unidentifiable remains were amply seen on excavated slabs in the field. Many of these fossils were discarded unless they were deemed to possess patterns or structures that might later be identified in the laboratory, and some of these were later identified (and included among faunal counts). Shell hash lenses and other items, which appear to have been part of (transported) death assemblages, were not included in the faunal counts (for further details, please see Devereux (2001)).

Metadata for each taxon were collected using a literature survey (see references section in 'metadata_traits.csv') for the following properties: taxonomic affiliation, habitat, size, motility and preservation potential. Taxonomic affiliation was noted only when there was a majority consensus for the affiliation across sources, otherwise these were omitted from the analysis. Size data were based on the maximum size of specimens found in literature. Motility and habitat were inferred from descriptions of each taxon's anatomical characteristics. The preservation potential assignments were primarily based on literature descriptions. Hard-bodied taxa are those with biomineralized skeletons, heavily-sclerotized parts, or decay-resistant organic cuticle. Intermediate-group taxa are those with light sclerotization or unsclerotized cuticle. Soft-bodied taxa are those with soft cellular outer layers and soft internal tissues. Enigmatic metazoans (i.e. for which we have no biomineralized/sclerotized preserved parts and have no phylum consensus) were assigned to the soft-bodied group.

Identifying sub-assemblages

We used ANOSIM (Analysis of Similarity: Clark and Warwick, 1994; Bonuso et al., 2002), and SHEBI (S (species richness)-H (information) -E (evenness) analysis for Biofacies Identification: Buzas and Hayek, 1998; Handley et al., 2009) to detect consensus biofacies or sub-assemblages in the sampled region. ANOSIM is a widely used non-parametric, distance-based clustering method. Based on the rank ordering of Bray-Curtis similarities (Clarke and Warwick, 1994), ANOSIM tests for differences in community structure by mixing permutation tests with a general Monte Carlo randomization approach (Hope, 1968). SHEBI recognizes edges between samples of specimens along a (spatial or temporal) transect. It depends upon the anticipated behavior of the evenness metric, which is associated with Shannon-Weaver information, as the number of samples within a single community rises (Handley et al., 2009). Here, each sample was a 10 cm layer of shale with abundance values for each taxon. Each method was conducted on 100 bootstrap simulations of abundance for each 10 cm shale layer. The consensus values from the runs, using both methods, were pooled together, and the mean was used to define the boundaries of the sub-assemblages (named A, B, C and D from oldest to youngest). ANOSIM and SHEBI were implemented using the *vegan* (Oksanen et al., 2019) and *foramsv2.0-5* (Aluizio, 2015) packages in R, respectively.

Agent based models

Agent based models (ABMs) provide an alternative to equation-based simulations for investigating ecological scenarios in a realistic way, along with providing an easy way to incorporate spatial dependence and heterogeneity. Properly implemented, ABMs provide results that match and complement existing ecological theories and experimental evidence (DeAngelis and Grimm, 2014; Karsai et al., 2016). This led to us to choose an ABM implementation over an equation-based implementation, for representing a simple toy model of multiple prey predator interactions. Given that we are dealing with a long term (averaged) ecological abundance dataset of multiple species, there are (i) no equivalent long term complex prey-predator census dynamics of equivalent settings, and (ii) actual prey-predator relations are can only hypothesized based on paleontological evidence (see Dunne et al., 2008), we decided to use a simple ABM implementation that would have as few assumptions as possible and at the same time, also been accepted to give dynamics that have been observed in theory and experiments of prey-predator interactions (Wilensky and Rand, 1997; Tobin and Bjørnstad, 2003; Liebhold et al., 2004; Blasius et. al., 2019).

This led us to use the NetLogo language (Wilensky and Rand, 1997) and extend a Lotka-Volterra prey-predator (wolf-sheep) base model in the NetLogo library, which replicates simple ecological phenomena among prey and predators (Wilensky and Rand, 1997), to create ABMs for purposes of (a) quantifying the impacts of preservation biases, (b) calculating prey-predator correlations, and (c) categorizing interactions.

The primary simulation involved 25 species, with 17 prey and 8 predators, and was based upon an extended implementation of the base Lotka-Volterra wolf-sheep model in the NetLogo library (Wilensky and Rand, 1997). All prey fed upon a common resource, which had two parameters attached to it – rate of resource regrowth and initial density of resources (relative to the total area, which was a 500x500 grid). The resource featured an energy content, as did the prey (all prey had equal energy content for simplification). Predators were assigned either a generalist or specialist feeding style. Generalists could eat all types of prey whereas a specialist could only eat one type of prey. Energy was necessary for reproduction, and for simplicity, at each reproduction event we divided the energy between the mother and the offspring, provided that the organism had enough energy to reproduce. The rate of reproduction was controlled as a variable. One million runs of the model were conducted that involved sweeping all parameters throughout their ranges using the Latin hypercube sampling method. Each model ran until it reached a stable state (only resource was left, all predators died, or all of the organisms died) or it reached 50,000 time points, whichever occurred first. Data were transferred to R for further processing using the

package *RNetLogo* (Thiele, 2017). Each of these models were used as a dataset for (a) testing bias, (b) calculating prey-predator correlations, and (c) categorizing interactions.

The second model was the same as the first/primary model except that each predator species was randomly assigned a different preference for each prey (between 0 and 1). This preference was the probability of a predator consuming a given prey when encountered. One million runs of the model were conducted that involved sweeping all parameters throughout their ranges. Each model ran until it reached a stable state (only resource was left, all predators died, or all of the organisms died) or it reached 50,000 time points, whichever occurred first.

The main reason for performing the ABM simulations was to obtain time series data pertaining to populations of various species, such that their relative fluctuations could tell us more about their trophic and competitive interactions. In other words, system stability or convergence in any form was not necessary for our model, but rather to reduce the computational time, we looked for states where it was no longer meaningful to continue the simulations to 50,000 iterations. The set of simulations that terminated early included cases where only resources persisted or where all species went extinct. From an initial pilot study, we saw a range of extremely complex patterns in populations, and observed slightly different outputs even with the same initial conditions. These results were due to the stochasticity inherent in our spatial ABM models, and we accommodated this variability by increasing the number of runs of the simulations.

To understand the effect of different parameters on the resultant correlations, as well as the effect of different lengths of time on the correlations, we performed partial rank correlation coefficient (PRCC) analysis in Figure S11. We ran 1 million simulations with different initial conditions and parameter settings based on a Latin hypercube sampling paradigm and observed the dependence of the final prey-predator correlation. We did not observe any strong dependence of pairwise correlations on initial conditions or parameter values except for the parameter controlling the preference/categorization (specialist or generalist) of the prey-predator pairs. A list of all the parameters and initial conditions are provided in Figure S11.

Data from all ABM simulations were transferred to R for further processing using the package *RNetLogo* (Thiele, 2017). Each of these models was then used as a dataset for categorizing interactions.

Constructing networks

Fossil count data from two adjacent 10 cm layers were combined in each sub-assemblage to increase species coverage for network construction. For each 20cm unit of each sub-assemblage (A through D, excluding A' and D' as in Figure 1 on the basis of preservation bias), we iteratively sampled fossils using bootstrap process for 1000 iterations. Using the data for each iteration, we calculated mean correlations between distinct 20 cm blocks for each sub-assemblage across all the bootstrap replicates. Given that some of these interactions can be spurious, we applied partial correlation corrections to the correlation matrices of each sub-assemblage (for details on partial correlation corrections in networks – see Epskamp and Fried, 2018). This ensured that when a third variable is associated with two measurements, after eliminating the effect of that variable, through partial correlation correction, we are able to provide robust estimate for association as compared to the existing raw correlation, i.e., this step corrects for spurious correlations arising from indirect effects (such as correlation between A and B because both are correlated with C). Next, we performed a Fisher Z-transform of the partial correlation matrices and calculated the probability of observing the estimated Z-scores by chance (based on a normally distributed null distribution). Finally, we used the Benjamini-Hochberg correction of p-values to eliminate those

interactions whose corrected correlation p-values exceeded 0.01. This yielded the final set of high-fidelity interactions for each sub-assemblage.

We also created networks on a running time-frame basis where we started at the beginning of the assemblage and repeated the process of network construction as described above for all possible 1.2 m sub-sections created by shifting the analysis frame in 20cm increments.

Pair-wise correlations were calculated for each dataset of the agent-based model simulations and across differently sized time steps as slices for calculating correlations (data were aggregated for each slice) (see Figure S2). We took 100 time-steps as the benchmark for each time slice for constructing networks for all purposes as the correlation saturated at a high enough value and the effects of phase difference and noise were reduced at this time scale of simulations.

Testing Preservation Bias using Exponential Random Graph Models

Exponential Random Graph Models (ERGMs: Holland and Leinhardt, 1981) are a preferred tool for evaluating how individual variables shape network structures. ERGMs have been used in the past to look at missing data and bias (Robins et al., 2004). We used the *ergm* (Handcock et al., 2019) package in R.

Using the trophic ABM datasets, we assigned each species in each simulated dataset to one of three preservation categories (α, β, or γ) to create a new 'partially preserved' dataset whose abundance values were adjusted downward by fixed preservation probabilities where

$$1 \geq P(\alpha) \geq P(\beta) \geq P(\gamma) \geq 0$$

These three categories can be thought of differential preservation categories: for example, in case of body type: hard bodied (preserves well like α), intermediate bodied (preserves decently but less than hard body, like β) and soft bodied (preserves poorly as compared to other body types; can be denoted by γ).

We repeated this procedure 100 times each for all 1 million simulated datasets and then constructed corresponding networks for each of the original and partially preserved datasets. For each of these constructed networks (both altered/partially preserved and original), we calculated the dependence of the network structure on the preservation category (α, β or γ) using ERGMs. We calculated the p-value resulting from the ERGM model for both the altered (partially preserved) networks and the original (intact) networks, as well as their mutual Hamming distance.

The bias coefficient (B) is measured in terms of these ERGM p-values of the original and partially preserved networks ($p_{original}$ and $p_{partially\ preserved}$ respectively) as

$$B = \frac{p_{original} - p_{partially\ preserved}}{p_{original}}$$

B > 0.5 on this scale corresponds to a change of ~0.2 of Hamming distance (Figure S3). Note that the ABM simulations were used to validate this statistical method before we applied it to the fossil data.

Moreover, this framework can detect biases in network structure based on categorizations, even when the relative preservation potentials among the categories is unknown, but only the categorizations are known. This is a useful property because, although we can assign relative ease of preservation in categorizations of say, body type – assigning the same for habitat and body size might be more complex (see supplementary file 'metadata_traits.csv').

Using this framework, we calculated ERGM p-values for each of the networks from the running time-frame analysis, as well as the four sub-assemblages (A-D) of the fossil data. Because we do not have the structure for the unaltered network of the fossil data (i.e. the actual abundance correlation networks from when the burial happened), we assume $p_{original} = 1.0$ for these analyses, in order to calculate the bias coefficient. This assumption gives an upper bound on the bias coefficient for our data, as the minimum possible ERGM p-value would be represented by $p_{original} = 1.0$ scenario (i.e. no dependence of network structure on any factor), but the actual p-value would usually be lower than this assumed value. As, all reported bias coefficients for the fossil data is based on this assumption, they represent the 'worst-case' values.

We performed three sets of analysis in this regard: body type, body size, and habitat affiliation. In each set, there were three categories, which were pre-determined (see supplementary file 'metadata_traits.csv' for details), according to available paleontological evidence. The body type categorizations were based on preservation or fossilization potential, as described in 'Data collection' sub-section of Methods – namely, hard bodied, soft bodied and intermediate, based on literature descriptions. Body size categorizations were <15 cm, 15 - 30 cm, > 30 cm maximum size. Habitat types were categorized into endobenthic/epibenthic, nektobenthic, nektonic/pelagic, based on literature survey (see references section in 'metadata_traits.csv').

Categorization of interactions and comparison with ABM

We subjected the distributions of abundance correlations to a maximum likelihood analysis to identify appropriate Gaussian basis functions. The mean, and standard deviation for a pre-defined number of Gaussian basis functions were determined using a general simplex-based optimization algorithm (Nelder and Mead, 1965). We compared results assuming 1 through 6 possible Gaussian basis functions and identified the optimal number of such functions for the correlation data using the likelihood-ratio test. All the scripts were implemented in R.

Once the number and nature of the Gaussians were estimated (for sub-assemblages A-D and for the running time-frame analysis), we used pairwise Kolmogorov-Smirnov (KS) tests between basis Gaussians to obtain a pairwise similarity matrix. The number of clusters of Gaussian basis functions was determined using spectral analysis based on the pairwise similarity matrix obtained from KS analysis and the gap statistic (Tibshirani et al., 2000). An advantage of using the gap statistic is that it does not pre-assume the number of required clusters (Tibshirani et al., 2000). All scripts were implemented in R using the package *cluster*. Four zones of clustering were determined using this method and are termed categories of interactions. Each category is shown in Figure 2 (a) using the range of all associated Gaussian means.

Next, from the ABM datasets, we identified the nature (i.e., generalist-prey, specialist-prey, competition, apparent competition) of all interactions whose partial correlations fell within ranges of the Gaussian mean clusters and plotted their relative occurrences in Figure 2c.

Consensus interactions were calculated from the running time-frame analysis and were defined as the high-fidelity interactions (or statistically corrected correlations) that stayed in the same interaction category for more than 50% of the time it occurred for a given pair of taxa. These results have been plotted in figures 3, S8 and S9.

Stochastic Block Models (SBMs) and Equitability analysis

The stochastic block model (SBM) is a tool, used to detect community structure in a network, where communities can be defined as multi-node subcomponents (or, blocks) of the network in which edges are more common within than between communities (Karrer and Newman, 2011).

We applied the framework of SBMs to the networks constructed from fossil data to understand the associations among species. In particular, we sought to understand whether the correlations on which those networks were built represented shared motility or habitat variables rather than species interactions. At each network level (which were calculated at a sub-assemblage level A-D and also at a fine time scale level), we used integrated classification likelihood (ICL) to calculate the number of clusters/blocks. On each block/cluster, we annotated the taxa in those blocks using the metadata on habitat and motility (separately; see supplementary file 'metadata_traits.csv' for details) and used the *mixer* package (Latouche et al., 2012) to find the distribution of annotated categories across blocks at a given network level. In order to numerically represent it, we calculated Shannon's equitability index (SEI), which is the normalized Shannon's diversity coefficient, based on the categories of habitat/motility for each block/cluster – and to estimate a network level (for a sub-assemblage/fine time scale analysis) average – we found the weighted average (on basis on number of taxa in each block/cluster) of SEI over all the blocks/clusters in the given network. We then plotted this average network SEI value at the fine scale analysis level in Figure S10(c).

SEI points at the dominance of a specific type of say, habitat/motility, on the taxa involved in interactions within a calculated cluster. If a given cluster is highly dominated by a single type of habitat/motility, SEI would be very low and would be 0 if it is only type. As SEI is normalized diversity index, the highest possible value of 1 occurs when all the types are equally probable. This is not the case with our fossil data – and hence, we calculated the maximum empirical value possible with the data (Figure S10(c)) for both habitat and motility separately. In addition, to make sense of how biased the correlational values are, we calculated the SEIs, for both habitat and motility, where a dominant type is equal to 95% of a given cluster and others are equally distributed in the remaining fraction (Figure S10(c)).

Supplemental References

Aluizio R. (2015). forams: Foraminifera and Community Ecology Analyses. R package version 2.0-5. https://CRAN.R-project.org/package=forams

Bonuso, N., Newton, C. R., Brower, J. C., & Ivany, L. C. (2002). Does coordinated stasis yield taxonomic and ecologic stability?: Middle Devonian Hamilton Group of central New York. Geology, 30(12), 1055-1058.

DeAngelis, D. L., & Grimm, V. (2014). Individual-based models in ecology after four decades. F1000prime reports, 6.

Epskamp, S., & Fried, E. I. (2018). A tutorial on regularized partial correlation networks. Psychological methods, 23(4), 617.

Fletcher, T. P., & Collins, D. H. (1998). The middle Cambrian Burgess Shale and its relationship to the Stephen Formation in the southern Canadian Rocky Mountains. Canadian Journal of Earth Sciences, 35(4), 413-436.

Handcock, M.S., Hunter, D.R., Butts, C.T., Goodreau, S.M., Krivitsky, P.N. and Morris, M. (2017). ergm: Fit, simulate and diagnose exponential-family models for networks. The Statnet Project (http://www. statnet. org). R package version, 3(0).

Handley, J. C., Sheets, H. D., & Mitchell, C. E. (2009). Probability models for stasis and change in paleocommunity structure. Palaios, 24(10), 638-649.

Holland, P.W. and Leinhardt, S. (1981). An exponential family of probability distributions for directed graphs. Journal of the american Statistical association, 76(373), 33-50.

Hope, A.C. (1968). A simplified Monte Carlo significance test procedure. Journal of the Royal Statistical Society: Series B (Methodological), 30(3), 582-598.

Karsai, I., Montano, E., & Schmickl, T. (2016). Bottom-up ecology: an agent-based model on the interactions between competition and predation. Letters in Biomathematics, 3(1), 161-180.

Latouche, P., Birmelé, E. and Ambroise, C. (2012), Variational Bayesian inference and complexity control for stochastic block models. Statistical Modelling, SAGE Publications, 12, 1, 93-115.

Nelder, J. A. and Mead, R. (1965). A simplex algorithm for function minimization. Computer Journal, 7, 308–313.

Oksanen, J., Blanchet, F. G., Kindt, R., Legendre, P., Minchin, P. R., O'hara, R. B., ... & Wagner, H. (2013). Community ecology package. R package version, 2(0).

Thiele J.C. (2017). RNetLogo: Provides an Interface to the Agent-Based Modelling Platform 'NetLogo'. R package v.1.0-4. https://cran.r-project.org/package=RNetLogo

Wilensky, U., & Rand, W. (2007). Making models match: Replicating an agent-based model. Journal of Artificial Societies and Social Simulation, 10(4), 2.